CHARACTERIZING THE ACTIVITY OF THREE NOVEL DIFFERENTIATION-INDUCING COMPOUNDS IN NEUROBLASTOMA CELLS

by

Alejandro Oviedo, B.S.

A thesis submitted to the Graduate Council of
Texas State University in partial fulfillment
of the requirements for the degree of
Master of Science
with a Major in Biochemistry
May 2020

Committee Members:

Liqin Du, Chair

Tania Betancourt

Alexander Kornienko

FAIR USE AND AUTHOR'S PERMISSION STATEMENT

Fair Use

Duplication Permission

DEDICATION

Todo mi trabajo se lo dedico a mi familia. En especial a mi hermanita, Samantha, y a mis abuelitos. Sin su apoyo no hubiese llegado a donde estoy hoy.

ACKNOWLEDGEMENTS

I would like to acknowledge my PI, Dr. Liqin Du, for the opportunity to grow and succeed as a scientist in her lab. I would also like to thank my lab mentor Dr. Zhenze Zhao for the countless and priceless advice that allowed me to progress with my experiments. Thank you to my lab mates, specifically Amy as we mentored each other through my time in lab.

To my cohort and friends, this journey would have been impossible without you guys always setting me straight and supporting me. Specifically, to Ari, Brianna, Julia, Kate, Yoshua, and Amanda. To my mentors Dr. Karen Lewis and Dr. Kevin Lewis, thank you for all the advice and support.

I would also like to thank the South Texas Doctoral Bridge Program for the guidance and support provided throughout these two years. Being part of this program has allowed to flourish and push myself to become a better scientist. Thank you so much to Dr. Blake, Dr. Oyajobi, Dr. Salinas, and Dr. Chang.

TABLE OF CONTENTS

Page

LIST OF TABLES

Table **Page**

LIST OF FIGURES

Figure **Page**

ABSTRACT

Neuroblastoma is the most common extracranial tumor in children. It makes up 8% of all childhood cancers and is the cause of 15% of all childhood cancer-related deaths. Neuroblastoma arises from neural crest precursor cells that fail to differentiate into mature neurons. The biggest threat for high-risk neuroblastoma patients is treatment-resistant relapse due to minimal residual disease. Current post-remission maintenance therapy includes the use of differentiation agent 13-cis-retinoic acid. However, approximately 50% of patients treated become unresponsive to this agent. The discovery of new differentiation agents is necessary in order to treat patients resistant to current available therapies. Using a high content phenotypic screening of a Chembridge small molecule library, three novel neurite-inducing small molecules (Compounds 3, 4, and 10) were identified. The objective of my study is to determine whether the hit compounds have a generic differentiation-inducing effect in neuroblastoma cells with different genetic backgrounds, and whether that the induced cell differentiation by these compounds is coupled with cell cycle arrest and apoptosis.

Our results demonstrate that treatment with compounds 3, 4, and 10 increase neurite outgrowth in BE(2)-C and KELLY cells. Compound 3 is validated to induce differentiation through at least two molecular differentiation markers in BE(2)-C, KELLY and CHLA-90 cells. It also has a generic effect on suppressing cell proliferation and decreasing cell viability generically. Western blot analysis, the differentiation

inducing activity of compound 4 is validated BE(2)-C and KELLY cells. Compound 4 also decreases cell viability and inhibits proliferation generically. Through an apoptosis assay, compound 4 induced apoptosis in BE(2)-C and KELLY cells. The differentiation inducing activity of compound 10 was validated in BE(2)-C, KELLY and CHLA-90 cells. Compound 10 decreased cell viability in cell lines BE(2)-C and CHLA-90, suggesting its activity might be cell-type specific. It inhibits proliferation in the four cell lines and induces apoptosis in BE(2)-C and KELLY cells.

In summary, my findings suggest that compound 3 is the best candidate out of the three hit compounds. Future investigations are needed to further characterize the differentiation inducing activity in multiple cell lines, the mechanisms of reducing cell viability, and effect on cell cycle distribution.

1. INTRODUCTION

1.1 Neuroblastoma

Neuroblastoma is the most common extra cranial solid tumor in children and infants. It makes up about 8% of all childhood cancers, 15% of all childhood cancer related deaths and is the primary cause of death in children between the ages of 1 to 5 years old. It stems from precursor cells of the sympathetic nervous system that fail to complete the differentiation process (**Figure 1,** adapted from[2]).[1-3]

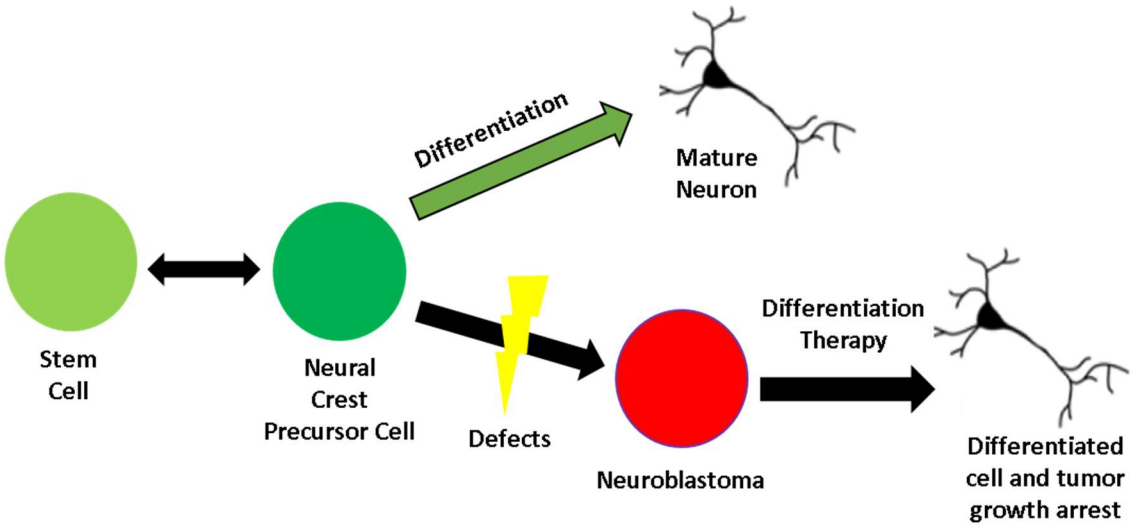

Figure 1. Schematic of neural crest development. Neural crest cells travel through the neural tube during embryogenesis and are destined to differentiate to mature neural cells that make up different parts the peripheral nervous system. Neuroblastoma stems from neural crest precursor cells that fail to complete the differentiation process. The precursor cell maintains stem cell characteristics allowing it to evade apoptosis and continue to proliferate. Differentiation therapy is used as a way to induce differentiation of immature tumor cell by targeting genes relevant to the differentiation pathway, leading to growth arrest and programed cell death.

It is widely recognized for its heterogeneity and extreme outcomes, from total tumor regression with minimal intervention to complete malignancy of the disease.[3-5] Tumors can arise anywhere in the sympathetic nervous system, which include the abdomen,

pelvis, neck, and thoracic regions.[3] Localization of tumors is also age dependent, where most infants get tumors in the thoracic and cervical regions. An estimated 65% of neuroblastoma tumors arise in the abdomen and more than half of these tumors are in the adrenal gland.[4] At time of diagnosis, about 50% of patients present with metastasized disease.[4] Neuroblastoma heterogeneity is a recognizable trait, which means that within one tumor there are cells that are derived from different neural crest lineages. These cells have different phenotypes, show distinct levels of tumorigenic potentials and malignancy, and are considered to be cancer stem cells.[6] It is because of this feature that neuroblastoma is infamously difficult to treat in high stages of the disease. The neural crest is described as a population of cells that are multipotent and can migrate.[7, 8] These neural crest cells arise from the dorsal surface of the neural tube during vertebrate embryogenesis. The cells travel through the neural tube and give rise to a variety of differentiated cells that form the sympathetic ganglia and adrenal medulla.[7, 8] During neural crest maturation the neural crest precursor cells obtain the ability of self-renewal and multipotent differentiation.[3] When this maturation process is inhibited or disrupted the precursor cells are likely to undergo programmed cell death because of their inability to make synaptic connections due to their immature status **(Figure 1)**[9] However, the expression of "pro-survival" factors, or oncogenes such as *MYCN* cause the neural precursor cells to evade apoptosis and extensively proliferate[3]. The disruption of this process at different stages is also thought to be the cause for the heterogeneity expressed by this disease **(Figure 2).**[3]

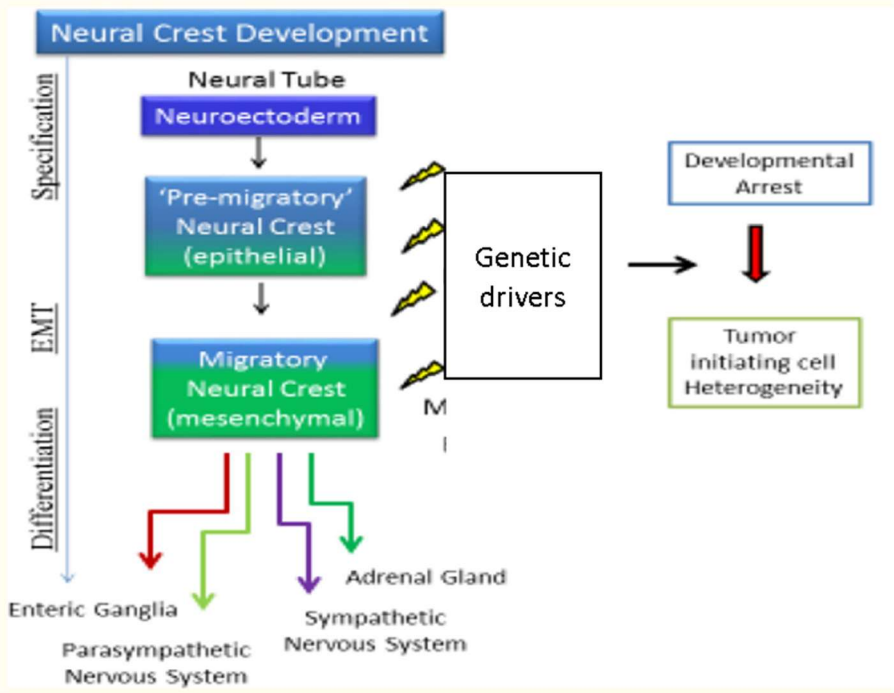

Figure 2. Neural crest development. Genetic factors disrupt the development of neural crest cells at different time points and this leads to neuroblastoma hallmark of heterogeneity. Image altered from reference.

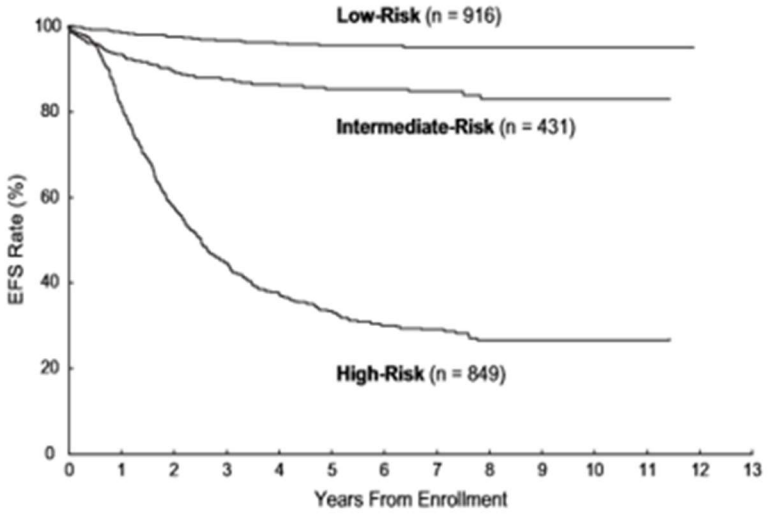

Figure 3. Event-free survival percentage by risk group. Low-risk and intermediate-risk neuroblastoma patients have better outcomes after achieving remission. High-risk patients have lower EFS due to relapse. Image obtained from reference.

1.2 Prognosis and treatments

Neuroblastoma patient prognosis can be predicted based on systems and guidelines set by the International Neuroblastoma Staging System (INSS) and the International Neuroblastoma Risk Group (INRG) staging system. In order to customize treatments and therapy, a risk assessment of the patient must be performed. This is done through age, stage of disease at time of diagnosis, *MYCN* status, DNA ploidy, and tumor histology classification.[5] With factors characterized the patients are grouped into low, intermediate or high-risk.[5, 10] Children with low-risk disease have a 95% to 100% event free survival (EFS) probability. Intermediate-risk disease patients have an 85% to 90% EFS probability. And patients in the high-risk group have less than a 40% EFS probability **(Figure 3).**[4, 5] Low and intermediate-risk patients can achieve remission with either minimal intervention or multiple rounds of chemo/radiotherapy. However, the treatment for high-risk neuroblastoma involves multimodal treatment: chemotherapy, surgery, radiotherapy, and biological agents (retinoids, etc.) along with newly added immunotherapy for post-remission care.[3, 4]

1.3 Differentiation therapy

Differentiation therapy is the stimulation of malignant cells to differentiate into their mature states in order to inhibit proliferation and undergo some form of programmed cell death, instead of using cytotoxic treatments to kill the cells directly and non-specifically **(Figure 1).**[11] This was thought of as a post-remission treatment to ensure remission without relapse.[11] The first supporting case for differentiation therapy was its use for acute promyelocytic leukemia using the Vitamin A derivative, all-*trans*-retinoic acid.[11] Standard care for post remission maintenance therapy for high risk neuroblastoma

is 13-*cis*-retinoic acid.[4] Retinoids are metabolites of Vitamin A that have been shown to induce cell growth arrest and morphological differentiation of multiple neoplastic cells.[12, 13] Retinoids, 13-*cis*-retinoic acid and All-*trans*-retinoic acid have been shown to inhibit proliferation in breast cancer, leukemia, embryonal carcinoma, and melanoma cells.[12] Retinoic acid (RA) is thought to mediate the expression of transcription factors by binding to retinoic acid receptors such as RAR and RXR **(Figure4).**[13] When retinoic acid binds to the receptors, the heterodimer undergoes a conformational change that allows it to bind to target sequences on DNA termed Retinoic Acid Response Elements (RARE).[13] It is thought that most neuroblastoma cell lines have RAR and RXR expression but that treatment with RA induces further expression of the receptors.[13] MYCN expression decreases with treatment of 13-cis-retinoic acid, and treatment also gets rid of malignant phenotype.[12, 13]

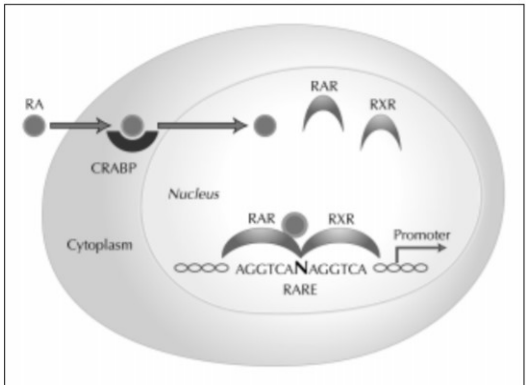

Figure 4. Mechanism of action for Retinoic Acid. Retinoic acid is transported into the cell where it binds to a cellular retinoic acid binding protein (CRABP). This CRABP then facilitates the movement of RA into the nucleus where it is released and can bind and dimerize RAR and RXR. The heterodimer then undergoes a conformational change that allows it to bind efficiently to DNA at a RA Response Elements. This is how transcriptions of certain genes are regulated by RA.

Although survival for high-risk neuroblastoma patients increases about 35% with 13-cis-retinoic acid treatment, the overall 5-year event free survival is still less than

50%.[14] Relapse remains the main problem with long term survival for high-risk patients. Patients older than 18 months, with higher stage of disease, *MYCN* amplification, unfavorable histopathology, and partial response to chemotherapy are at higher risk of poor prognosis.[14] Therapy-resistant relapse has been hypothesized to happen due to the tumor-initiating cells (TIC) or cancer stem cells (CSC) that harbor stem-like properties, such as self-renewal, pluripotent differentiation, and the expression of multi-drug resistant proteins (MDR) and ATP-binding cassette (ABC) transporter proteins.[15-17] A subset of stem cells called side population have been identified in mammalian tissues and are known to maintain a high efflux for mitotic drugs. Such export of drugs and the ability of these TIC to undergo self-renewal is a possible factor for therapy-resistant relapse.[15] In fact, a side population of these cells was found in 65% of primary neuroblastoma samples as well as in cell lines resistant to chemotherapeutic agents.[18-20] Therefore, it is important to continue investigating differentiation pathways and to continue searching for ways to improve differentiation therapy along with the identification of new differentiation agents that can have additive effects with RA or surpass its effectiveness.

1.4 Small molecule libraries and differentiation agents

Small molecules have been found to control stem cell fate, differentiation, and proliferation.[21] High-throughput screenings (HTS) are a fast and efficient way of finding hit compounds from small compound libraries that contain hundreds or thousands of potential hits.[22, 23] New ligands for enzymes or receptors can be found by screening compound libraries. Once a hit molecule is identified it can then serve as a template for modification in order to alter and improve binding or function.[22, 24] There are different

types of small molecule screenings (such as virtual docking screenings, HTS, etc.) that can lead to the discovery of anti-cancer agents.[25-27] Small molecule screenings have been successfully used to provide differentiation agents in previous cancer studies. One example is a screening that was performed with 330,000 small compounds using a high-throughput flow cytometry phenotypic screening. From the 330,000, 29 hits demonstrated potential in overcoming differentiation arrest in acute myeloid leukemia.[28] Similar to this article, our group performed a high-content phenotypic screening (HCS), using neurite outgrowth as a marker, of a 10,000 compound small synthetic molecule library from Chembridge on neuroblastoma cell line BE(2)-C. And we were able to identify three hit compounds that induced morphological differentiation on BE(2)-C cells **(Figure 5)**.

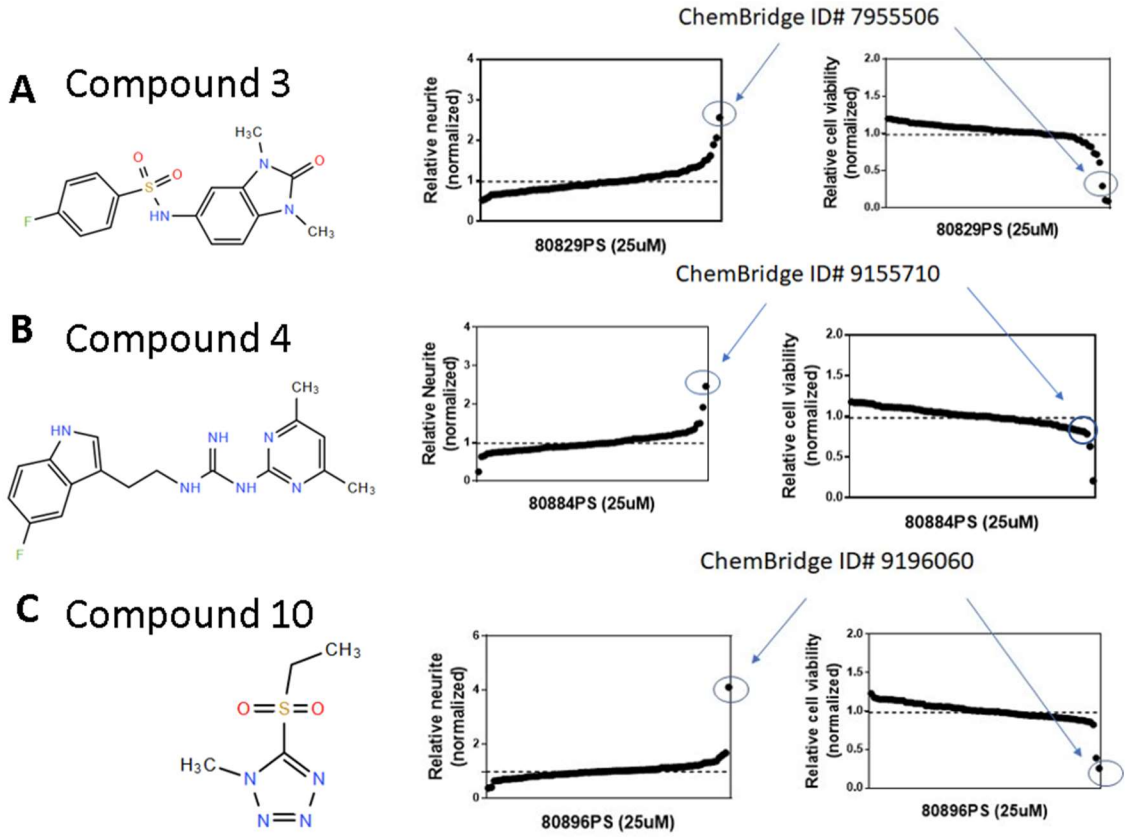

Figure 5. Hit compounds: relative neurite outgrowth and relative cell viability. A high-content phenotypic screening was performed on a 10,000 small synthetic compound library. Panel A, B, and C are the results from the screening. Each panel has the hit compound circled. These are the preliminary results that lead to this project.

1.5 Cellular responses of neuroblastoma cells to differentiation agents

Knowing the cellular responses to anti-cancer agents is important to predict the outcome of any therapy. For example, cancer cells induced into quiescence state but not into the final death pathways are likely to resist further drug treatment and cause tumor relapse. This could be due to the cells being able to reenter the cell cycle and evade cell cycle arrest.[29] Knowing whether a differentiation agent will induce cell cycle arrest, and which pathways it prefers can determine the effectiveness of the agent and or therapy. Cell cycle withdrawal or G0 phase has three subtypes known as quiescent, senescent, and

differentiated **(Figure 6)**. Quiescent is characterized as reversible cell cycle withdrawal. It is also preferred by progenitor cells when induced to stress in order to avoid complete withdrawal. Cell senescence and terminal differentiated states are both irreversible and tend to be the goal of most therapies.[30] Cellular response induced in neuroblastoma cells due to differentiation agents aside from RA have not been systematically investigated. RA is known to cause G1 cell cycle arrest. However, there is also evidence of cell senescence being one of the pathways by which growth arrest is achieved after treatment.[31] It has also been stated that RA inhibits proliferation through differentiation of cells rather than the activation of programmed cell death pathways.[32-34] This means that even though growth is arrested some cells may only achieve a quiescent state and be able to reenter the cell cycle after removal of treatment.[31] The above demonstrates the importance of studying the cellular response of neuroblastoma cells to differentiation agents, in order to further understand the mechanisms that control cell fate in neuroblastoma.

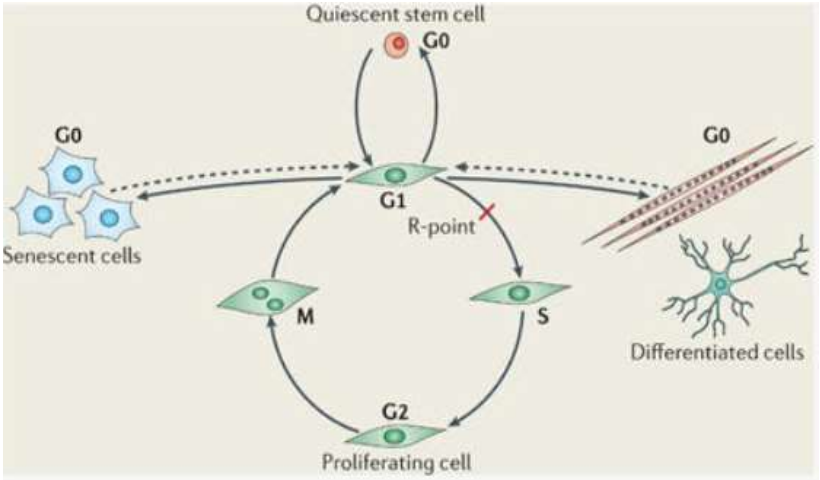

Figure 6. Cell cycle with three types of G_0 phase. Withdrawal from the cell cycle leads to G0 phase. This could be due to defective cells with DNA damage, which become senescent cells. Quiescent cells usually withdraw reversibly to avoid stress and preserve themselves. Differentiated cells exit the cell cycle phase since they have obtained their function. The dotted arrows are due to observed reversal of 'irreversible" pathways, however it is only under extreme conditions for senescent cells. This demonstrates how anti-cancer drugs can have variability in their success to cause growth arrest.

1.6 Research objectives and specific aims

The main goal of my study is to determine if compounds 3, 4 and 10 have a generic differentiation-inducing effect on neuroblastoma cell lines, and if the induced cell differentiation is coupled with cell cycle arrest and apoptosis. My proposed aims are as follows:

Aim 1: Validate the differentiation-inducing activity of the three compounds in multiple neuroblastoma cell lines by measuring neurite outgrowth and expression of differentiation markers. This will be done through a neurite outgrowth assay using NeuroTrack software on images obtained by the Incucyte. Expression of molecular differentiation markers, including non-specific enolase (NSE), growth associated protein

43 (GAP43), and β-Tubulin III, and Chromogranin A (CHGA), will be observed by western blot.[35]

Aim 2: Determine whether the compounds have a generic effect in reducing cell survival in multiple neuroblastoma cell lines. Cell viability is measured via an MTT assay for each cell line and a colony formation assay is performed to observe effects of compounds on clonogenicity.

Aim 3: Investigate the cellular mechanisms by which the compounds induce cell death, by determining their effect on cell cycle distribution and cell apoptosis. Cell cycle analysis will be performed through DNA content quantified by DAPI intensity using Lionheart LX Automated Microscope.[31, 36] In order to investigate the cellular mechanisms by which the compounds induce cell death, an apoptosis assay utilizing CellEvent™ Caspase-3/7 Green Detection Reagent.[37, 38]

Asides from the above aims, my other interest is to investigate whether the three compounds induce neuroblastoma cell senescence. Although this is not within the scope of my thesis proposal, I will present my preliminary investigations in the end of this thesis paper.

2. MATERIALS AND METHODS

Table 1. List of materials and equipment used in this study. Shown are the items, names of companies from which the items were purchased, locations of the companies, and the catalog numbers of the items.

Materials	Companies	Location
EquaFetal Bovine Serum/ 0.1 micron filtered	Atlas Biologicals	Fort Collins, CO
Pen Strep [+] 10,000 U/mL Penicillin [+] 10,000 ug/mL Streptomycin	Life Technologies	Carlsbad, CA
0.05% Trypsin, 0.53 mM EDTA, 1X [-] NAHCO3	Corning	Manassas, VA
DMEM 1X w/ L-glutamine	Corning	Manassas, VA
Calnexin polyclonal antibody (1mg/mL)	Thermo Fisher	Waltham, MA
Neuron Specific Enolase Rb mAb to NSE	Abcam	Cambridge, UK
GAP43 Rb pAb to GAP43	Abcam	Cambridge, UK
Beta Tubulin III Rb pAb to Neuron Specific Beta Tubulin III	Abcam	Cambridge, UK
Goat anti-rabbit IgG (H+L) secondary ab, HRP	Thermo Fisher	Waltham, MA
Rabbit anti-CHGA	Cell Signaling	Danvers, MA
TrkA (12G8) Rabbit mAb #2510	Cell Signaling	Danvers, MA
Cleaved PARP (Asp214) Rabbit mAb	Cell Signaling	Danvers, MA
Supersignal West Pico PLUS Chemiluminescent substrate	Thermo Scientific	Rockford, Il
Acrylamide/ Bis-(29:1) 40% Soln	Alfa Aesar	Wardhill, MA
PlusOne TEMED	GE Healthcare Life Sciences	Pittsburgh, PA
Dimethyl Sulfoxide BP231-1	Fisher Bioreagents	Pittsburgh, PA
Tween 20 Acros Organics	Aros Organics	Waltham, MA
Resolving Buffer Tris base 1.5 M, pH 8.8 and SDS 0.4%	Boston Bioproducts	Ashland, MA
Stacking Buffer Tris base 0.5 M, pH 6.8 and SDS 0.4%	Boston Bioproducts	Ashland, MA
Transfer Buffer 10X Tris/Glycine 0.25 M Tris-1.92 M Glycine	National Diagnostics	Atlanta, GA
Running Buffer 10X Tris/Glycine/SDS 0.25 M Tris- 1.92 M Glycine- 1% SDS	National Diagnostics	Atlanta, GA
Non-fat Powedered Milk	Boston Bioproducts	Ashland, MA
Pierce BCA Protein Assay Kit	Thermo Fisher	Waltham, MA
Bluestain Protein Ladder	GoldBio	St. Louis, MO
Spectra Multicolor Broad Range Protein Ladder	Thermo Scientific	Rockford, Il
Pierce Protease Inhibitor mini tablets EDTA-free	Thermo Scientific	Rockford, Il
Tris Base	Fisher Scientific	Fairlawn, NJ
3-(4,5-Dimethylthiazol-2-yl)-2,5-diphenyltetrazolium bromide (MTT) ≥98%	Thermo Scientific	Rockford, Il
DPBS w/o calcium & magnesiym	Corning Cellgro	Manassas, VA
Triton X-100	Fisher Scientific	Fairlawn, NJ
PVDF Transfer Membrane 0.45 uM 26.5 cm X 3.75 m roll	Thermo Scientific	Rockford, Il
100 mm Cell Culture Plates	Corning	Manassas, VA
60 mm Cell Culture Plates	Corning	Manassas, VA
96-Well Cell Culture Plates	Corning	Manassas, VA
Molecular Devices SpectraMAX190 90-250V 50-60 Hz	Molecular Devices	Sunnyvale, CA
Canon CanoScan 900F MarkII	Canon	Ota, Tokyo, JP
SoftMaxPro 5.4.1 1992-2010	Molecular Devices	Sunnyvale, CA
Forma Series 3 Water Jacketed CO2 incubator Mod 4110	Thermo Scientific	Merietta, OH
Incucyte Zoom	ESSEN Bioscience	Ann Arbor, MI
Culture Hood 1300 Series A2 Mod 1307	Thermo Scientific	Merrieta, OH
CellEvent™ Caspase-3/7 Green Detection Reagent	Thermo Fisher	Carlsbad, CA
Lionheart FX	BioTek Instruments	Winooski, VT
ChemiDocXRS+System	BioRad	Hercules, CA
Graphpad Prism	Graphpad Software	La Jolla, CA
ImageJ	NIH	Bethesda, MD

2.1 Cell culture

Cells are cultured using 10% EquaFetal Bovine Serum (EFBS) and 1% Penicillin Streptomycin antibiotic supplemented DMEM. Cells were split every 3-4 days depending usually at a confluence of 80% or more. Media is removed and cells are washed with DPBS. To detach cells, 0.05% trypsin/ 0.53 mM EDTA was used at volumes of 400 uL for 60 mm plates or 900 uL for 100 mm plates. Cell are pelleted at 300 rcf for 3 minutes, and resuspended using fresh media warmed to 37˚C by heat bath, and seeded at preferred concentration in 3 mL of 37˚C fresh media for 60 mm plates and 12 mL 37˚C fresh media for 100 mm plates. Cells are kept in the Forma Series 3 Water Jacketed CO_2 incubator at 5% CO_2 and 90 % relative humidity. Cells used for experiements are only passaged 15 times before discarding, this is to prevent accumulation of mutations and to maintain healthy cells.

To find concentration of cells a hemocytometer is used to count cells in stock suspension of cells. From stock, 10 μL are removed and diluted in 40 μL of DPBS for a 5 fold dilution, 10 μL are then loaded onto the hemocytometer. After the counting of cells in 16 square peremeter, this value is multiplied by 5 for the dilution, and then 10 to obtain number of cells per microliter.

2.2 Cell lysate collection

Cells are scrapped from the plate in 10 mL of media, this solution is decanted into 50 mL conical tubes. Tubes are then spun down at 200 rcf for 5 minutes. Media is disposed of without distrubing cell pellet. Cells are resuspended using 0.5 mL of 1X Tris-Buffered Saline and transferred to 1.5 mL microcentrifuge tube. Cells are spun down at

300 rcf for 3 minutes, and supernatant is removed, and cells are washed again with 1X TBS. After final wash, cells are resuspended in 50-120 µL of lysis buffer depending on pellet size and placed in ice for 10 minutes. Cell lysates are then spun down at max speed for 5 minutes. Supernatant is transferred to new 1.5 mL microcentrifuge tube. For BCA assay, 5 µL of BCA standards are used (0, 25 µg, 125, 250, 500, 1000, 1500) and 2 µL of samples are used to find concentration of cell lysate. Samples were mixed with Solution A and Solution B (50:1) from the Pierce BCA Protein Assay Kit. Microplate reader measured asorbances at 562 nm. Concentration is calculated from fitted line obtained from BCA standards, multiplied by 0.8 and 2.5 for dilutions. Once concentration is calculated, ¼ of cell lysate volume of 5X protein ladder buffer is added to cell lysate. Proteins are denatured in heating block set to 90˚C for 5 minutes. Cell lysate is stored in -20˚C freezer for future uses.

2.3 Western blots

Gels were made using 8% or 10% acrylamide. Gels were loaded onto cassette holder and placed in electrophoresis rig. The rig was then filled with 1X running buffer (0.25 M Tris, 1.92M glycine, 1% SDS). For calnexin detection , enough volume was added to contain 5 µg of protein. For other proteins 10-20 µg was loaded onto wells. The SDS-PAGE ran at 120 volts for 50 minutes to allow samples to resolve. For transfering proteins from gel to PVDF membrane, the PVDF membrane was soaked in methanol for 15 minutes followed by diH_2O for the remining time. Once the SDS-PAGE was done running, the gel was removed from the plates and placed on top of membrane. The gel and membrade were sandwiched between two pads and sponges and then placed in

transfer rig along with an ice pack. For one membrane the transfer ran at 150 mA for 90 minutes, for two membranes the transfer ran at 200 mA for 120 minutes.

After electronic transfer, membranes are removed from sandwich, labeled, and placed in 5% dry milk TBST blocking solution for 1 hour. The membranes were then washed three times with 1X TBST. For the Calnexin blots, the membranes were incubated in 1:1,000 rabbit anti-calnexin primary antibody overnight. For NSE blots, the membranes were incubated in 1:1,000 rabbit anti-NSE primary antibody overnight. For CHGA blots, the membranes were incubated in 1:1,000 rabbit anti-CHGA primary antibody overnight. For PARP blots, the membranes were incubated in 1:1,000 rabbit anti-cleaved PARP primary antibody and 2.5% dry milk 1XTBST solution overnight. For overnight, the blots were stored in containers with lids in their perspective solutions in 4˚C fridge. After incubation with primary antibody, the membranes were washed three times with 1XTBST, and then incubated with secondary goat anti-rabbit conjugated with horseradish peroxidase (HRP) for 1 hour at room temperature. After incubation period, the membrane was washed three times using 1X TBST. The SuperSignal West Pico/Dura Chemiluminescent Substrate was made and the membranes were placed in the solution and immediately imaged. To image the ImageLab Software was used connected to the ChemiDocXRS+ system. The Hi-Resolution Chemi Luminescence mode for detection of protein bands and the Colorimetric mode for the ladder.

For re-blotting the PVDF membrane for a second protein, membranes were placed in menthol for 5 minutes to make them hydrophillic. They were washed with 1X TBS-T before incubating in 5% dry milk 1X TBS-T blocking buffer. Same steps were followed as regular blotting process.

2.4 Neurite outgrowth

Dilution plate was made in a 96-well plate, compounds were dissolved in DMSO. For neurite outgrowth experiements, compound concentration in the wells ranged from 100 μM to 0.15 μM. Compounds and DMSO control were added to 96-well plates prior to adding cells and culture media. Cells were trypsonized and collected once they reached 80% confluency in a 100 mm plate. Cells were resuspended and counted using a hemocytometer. Treatments lasted 4 days, on the fourth day the plates were imaged at 20X using the ZOOM Incucyte Imaging System. Neurite outgrowth was analyzed usisng Neuro Track Software and normalized to DMSO control. Neuro Track Software has definitions previously set that are used to analyze results, enuring that the definition chosen for metrics is appropriate for each cell line. An two-tailed t-test was performed on each concentration value with DMSO control.

2.5 MTT cell viability assay

Cells were treated with compound concentrations ranging from 100 μM to 0.15 μM. Compounds were added to a 96-well plate prior to the addition of cells. The number of cells per well were the same as neurite outgrowth. Once cells were imaged, the media was disposed of and MTT solution at a concentration of 2.5 μM/ μL. The cells were incubated for 4-6 hours. After incubation they were spun at 200 rcf in the 96-well plate for 5 minutes, the media was decanted and 100% DMSO was added to the wells. Plates were read using the SpecMax at wavelengths 630 nm and 570 nm[35, 39]. The values were subtracted from eachother and normalized to DMSO control.

2.6 Colony formation assay

Cells were plated in 100 mm dishes with 10 mL of 20% EFBS culture media, seeding density varied per cell line. Compounds were added the same day. Triplicates were done for each treatment and allowed to grow for 12 days, replenishing once throughout the 12 days. After 12 days, media was diposed of, cells were washed with 1X TBS twice. Crystal violet solution was added to the plates to stain the colonies of cells, for an incubation period of 15 minutes. Plates were washed using diH_2O to remove any residual crystal violet and air dried. Once dry, plates were imaged using Canon scanner. The images were analyzed using ImageJ.

2.7 Apoptosis live imaging using CellEvent™ Caspase-3/7 Green Detection Reagent

Treatments are added to 96-well plate for 12.5 μM and 25 μM. 1,500 cells per well are plated with full media. After 4 days of treatment a solution containing DPBS, FBS, and the CellEvent™ Caspase-3/7 Green Detection Reagent was made for a final concentration of 4 μM, and then added to treatment wells. Cells were imaged after 30 minutes using the Incucyte Phase & Green mode.

2.8 Cell cycle analysis Lionheart FX

A549 cells were plated in 60 mm dishes for 4 days. After 4 days of incubation the cells were fixed with 100% methanol, and stained with a 1:10,000 dillution of DAPI stianing. Plates were maintained in the dark, and imaged using the Lionheart FX microscope. Parameters were set according to cell size on the software, cells were imaged at 20X and 40X magnification. DAPI intensities were recorded at 20X magnification. Number of cells per intensity were graphed using Graphpad.

2.9 Senescence-Associated β-Galactosidase activity assay

KELLY cells were plated in 60 mm dishes for 6 days and their respective treatments. After 4 days of incubation the cells were fixed with 4% paraformaldehyde in PBS buffer for 1 minute. Fresh staining solution containing 40 mM citric acid/Na phosphate buffer, 5 mM $K_4[Fe(CN)_6]$ $3H_2O$, 5 mM $K_3[Fe(CN)_6]$, 150 mM sodium chloride, 2 mM magnesium chloride and 1 mg/ ml X-gal in distilled water was made. Cells were stained for 16 hours at 37˚C, washed with 1X DPBS, and stained with 1:10,000 DAPI solution for 30 seconds with a final wash with 1X DPBS. Plates were kept in the dark and imaged at 4X using color brightfield and DAPI detection on the Lionheart FX microscope.

3. RESULTS

3.1 Dose-dependent effect of compounds 3, 4, and 10 on neurite outgrowth in neuroblastoma cell lines

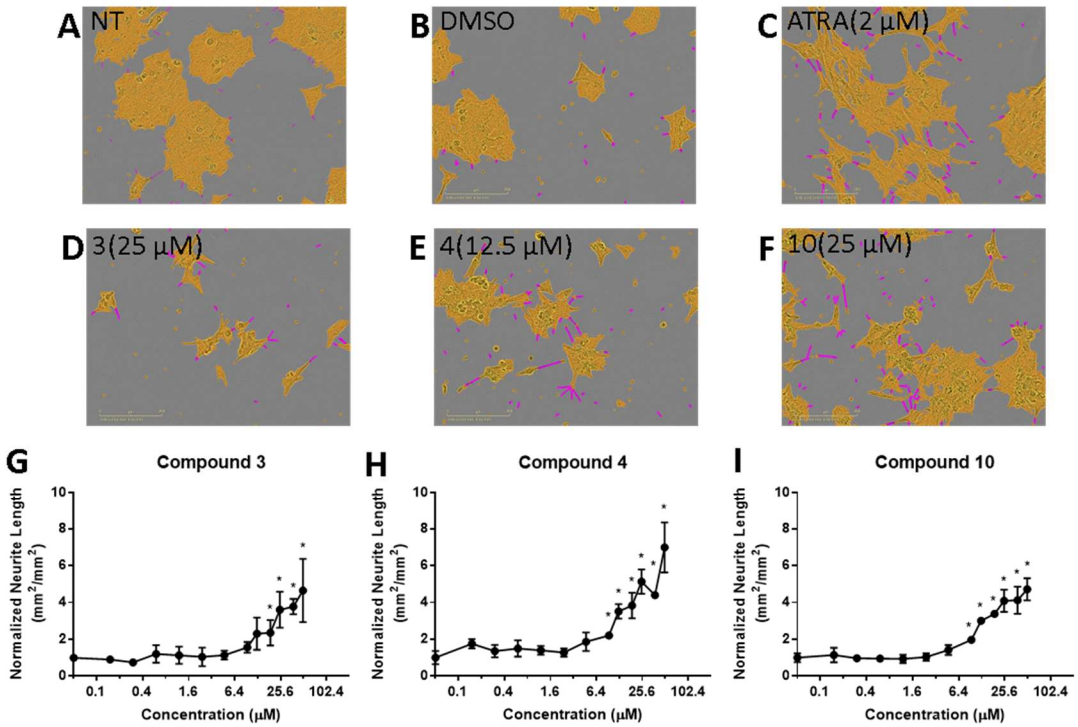

Figure 7. **Neurite lengths after treatment with compounds in BE(2)-C.** 1,000 cells per well were plated in a 96-well plate, triplicates were done for each concentration ranging from 0.15- 50 µM. **A-F** Show representative images from wells for each treatment. Images show cell clusters in yellow and neurite projections in purple.(NT= No Treatment) **G-I** After 4-day incubation with treatment, plates were imaged, and neurites were measured and normalized to DMSO control. *p< 0.05

As mentioned previously in **Figure 5**, the two markers that were used to screen through the 10,000 small molecule library were relative neurite lengths and relative cell viability in cell line BE(2)-C. The phenotypic change in BE(2)-C cells lead to further investigation of neurite outgrowth at different concentrations. All-*trans*- retinoic acid (ATRA) is being used as a positive control, while DMSO is considered a negative control in the results. In **Figure 7 A-F**, neurite projections are shown in purple and cell clusters

in yellow. Treatment with ATRA and compounds 3, 4, and 10 show an increase in neurite projections per cell cluster compared to DMSO. **Figure 7 G-I** are the quantifications of neurite length of the three treatments normalized to the negative control. Generally, as concentrations of the compounds increases, the neurites increase. Compound 3 has a significant increase in neurites starting at a concentration of 18.75 µM. Compounds 4 and 10 do not show a significant increase until a concentration of 9.4 µM. It should be noted that the number of live cells decreases past 50 µM for compound treatments.

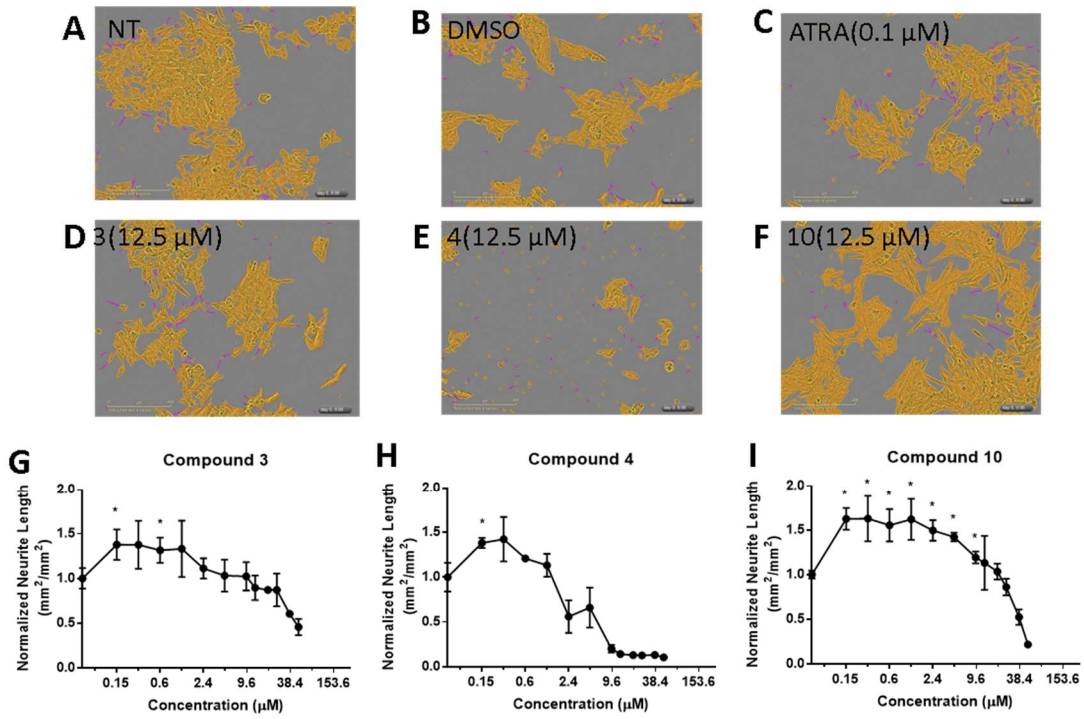

Figure 8. Neurite lengths after treatment with compounds in KELLY cells. 2,000 cells per well were plated in a 96-well plate, triplicates were done for each concentration ranging from 0.15- 50 µM. **A-E** Show representative images from wells for each treatment. Images show cell clusters in yellow and neurite projections in purple. **G-I** After 4-day incubation with treatment, plates were imaged, and neurites were measured and normalized to DMSO control. *p<0.05

Neurite Outgrowth was also investigated in the KELLY cell line, **Figure 8A-F** are representative pictures demonstrating the phenotypic changes induced by compound

treatment after 4 days. As shown in **Figure 8A** and **8B**, Kelly cells have small neurite projections visible without any treatment and with the negative control, DMSO. **Figure C** shows that the treatment with 0.1 μM ATRA induces visible neurite outgrowth. **Figure D-E** shows that treatments with the three compounds result in visible but not dramatic increase comparing with control. **Figure 8 G-I** shows the quantitative results of neurite length normalized to DMSO control with increasing concentration for each. KELLY cells rarely survived at concentrations greater than 25 μM. Neurite length for compound 3 increases from concentration 0 to 0.15 μM, maintaining the increase to 0.6 μM before steadily decreasing. Compound 4 shows a significant increase in neurite length for 0.15 μM, with a steeper decrease in neurite length. Compound 10 has a longer range from 0.15-9.6 μM where neurite lengths are increased compared to DMSO treatment.

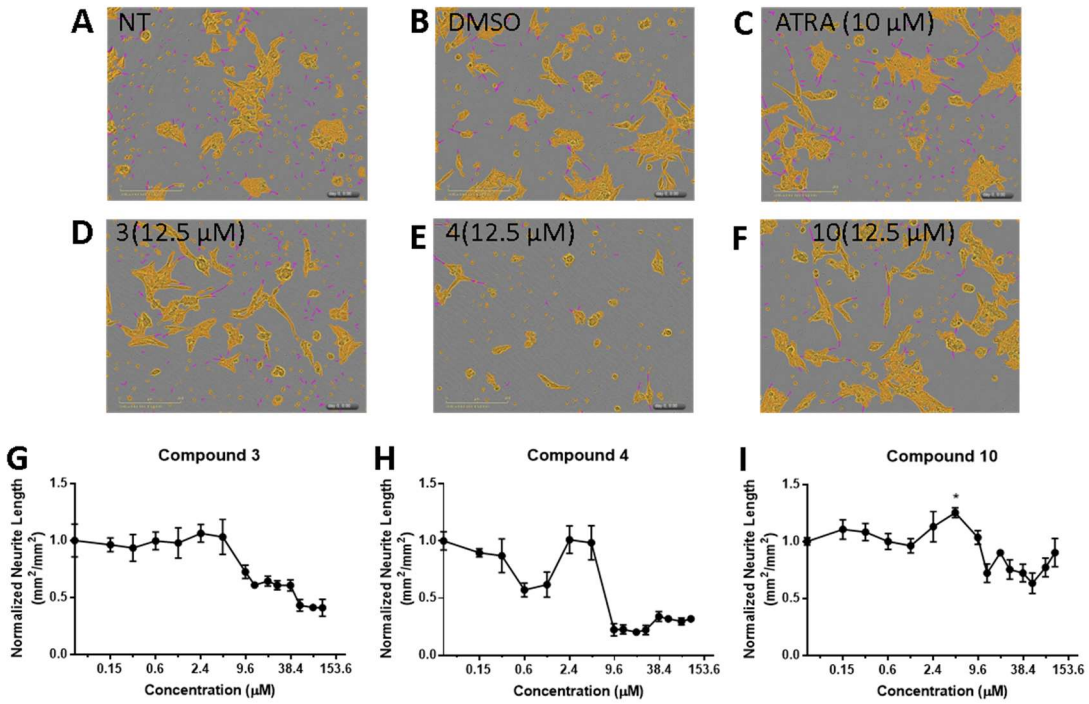

Figure 9. **Neurite lengths after treatment with compounds in *CHLA-90* cells**. 3,000 cells per well were plated in a 96-well plate, triplicates were done for each concentration ranging from 0.15 - 100 µM. **A-F** Show representative images from wells for each treatment. Images show cell clusters in yellow and neurite projections in purple. **G-I** After 4-day incubation with treatment, plates were imaged, and neurites were measured and normalized to DMSO control.

The neurite outgrowth assay was also performed in CHLA-90 cells, with concentrations ranging from 0.15-100 µM. **Figure 9A-F** shows representative images from each treatment. As seen in **Figure 9A-B** CHLA-90 cells are negative controls and have the neuroblastic phenotype with neurite projections already visible and quantifiable, therefore the main difference seen from **Figures 9D** and **9E** is a decrease in number of live cells comparing to control. **Figure 9G-I** shows the quantification of neurite lengths normalized to DMSO control, as concentration increases. For compound 3 neurite length stays the same from 0.15-4.7 µM, before steadily decreasing. Compound 4 shows a general decrease in neurite lengths due to small number of viable cells with quantifiable

neurites. The two points at 2.4 µM and 4.7 µM appear to be outliers compared to the points preceding and succeeding them. Compound 10 shows slight decline as concentration increases and has one significant concentration, 4.7 µM where neurite length exceeds DMSO control significantly.

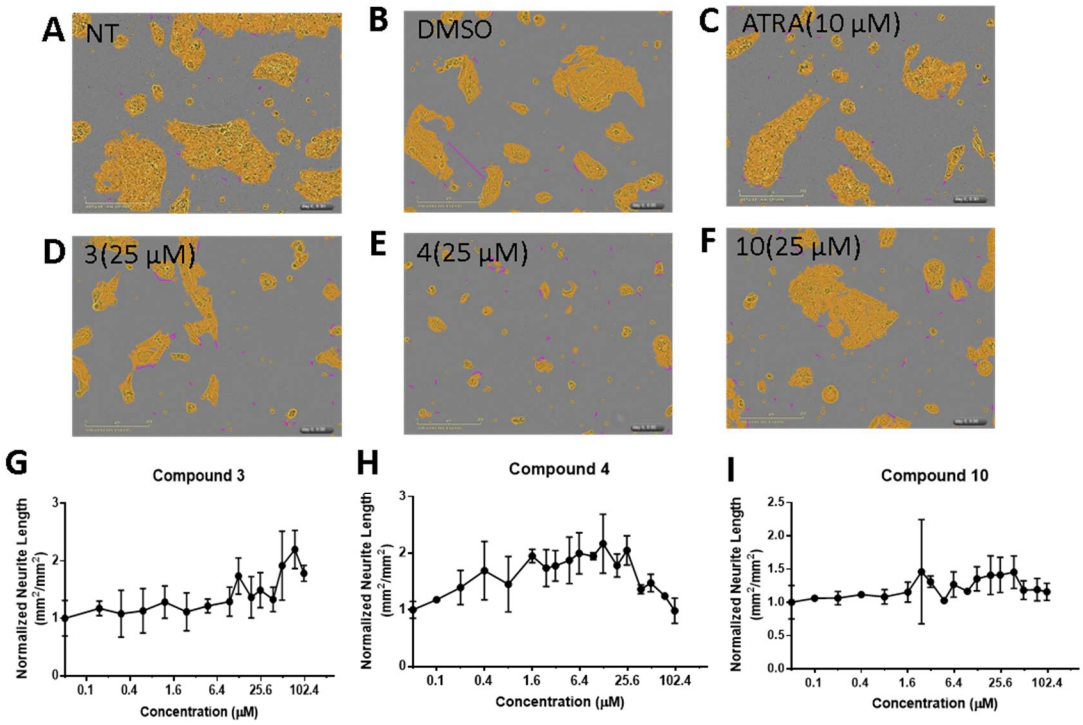

Figure 10. **Neurite lengths after treatment with compounds in SK-N-AS cells.** 1,000 cells per well were plated in a 96-well plate, triplicates were done for each concentration ranging from 0.15 - 100 µM . **A-F** Show representative images from wells for each treatment. Images show cell clusters in yellow and neurite projections in purple. **G-I** After 4-day incubation with treatment, plates were imaged, and neurites were measured and normalized to DMSO control.

The same neurite outgrowth assay was performed in SK-N-AS cells. **Figure 10A-F** shows representative images from each well and treatment. As demonstrated in the images, there are no neurite projections stemming from the cluster of cells in any treatment. Images also show that the NeuroTrack software is counting debris and outer edges of the cell's matrix as neurites, therefore **Figure 10G-I** are not quantifying the

actual neurite lengths. The standard deviations are large, showing inconsistency and lack of a trend. Cells remain clustered at different concentrations with no phenotypic change.

3.2 Effect of the three compounds on expression of neuronal differentiation markers

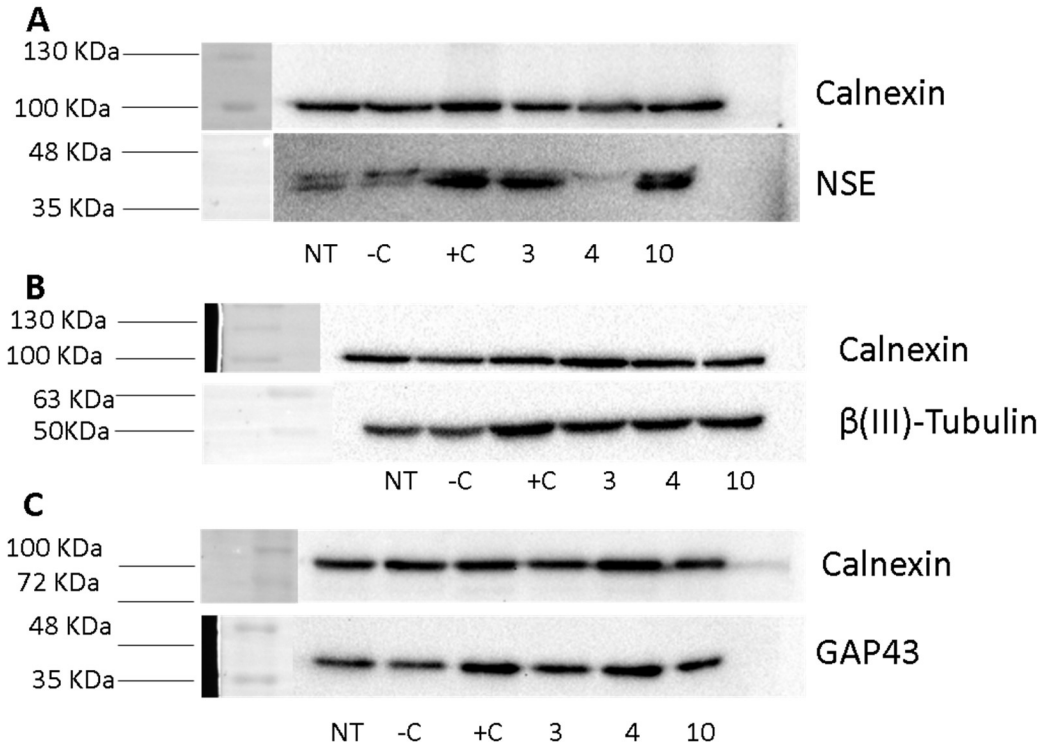

Figure 11. Expression of NSE, β(III)-tubulin, and GAP43 in BE(2)-C cells after treatment. A Shows the expression of Neuron Specific Enolase (~45 KDa) after 4-day treatment with compounds. Cell lysate was loaded at a concentration of 15 µg per well. **B** Shows expression of β(III)-Tubulin (55 KDa) after 4-day treatment with compounds. Cell lysate was loaded at 5 µg. **C** Shows expression of GAP43(43 KDa) after 4-day treatment. Cell lysate was loaded at a concentration of 5 µg. Cells were treated with a concentration of 25µM for each compound and 10 µL for DMSO control. Cell lysates were collected per treatment and stored at -20ºC. Calnexin (90 KDa) was used as a loading control and loaded at a concentration of 5 µg per well. NT= No Treatment, -C= DMSO (negative control), +C= ATRA (positive control), 3= Compound 3, 4= Compound 4, 10= Compound 10.

As part of Aim 1, expression of neuronal differentiation markers was investigated in order to validate whether compounds 3,4 and 10 have differentiation-inducing activity.

Figure 11 demonstrates the results from the investigation of neuronal differentiation markers in BE(2)-C cells after 4 days of treatment with compounds. **Figure 11A** shows the expression of differentiation marker Neuron Specific Enolase (NSE) at around 45 KDa. The double bands are most likely due to pre- or post-translational modifications that alter the KDa. There is an increase in expression of NSE in cells treated with ATRA(+C) as expected, since ATRA is known to induce differentiation. There is also a dramatic increase in expression of NSE in cells treated with compounds 3 and 10. Compound 4 has less expression than cells with no treatment (NT) and cells treated with DMSO (-C). **Figure 11B** demonstrates the expression of differentiation marker β(III)-Tubulin at 55 KDa, after 4 days of treatment. No treatment (NT) cells and DMSO (-C) treated cells have a lower expression of β(III)-Tubulin. ATRA(+C) treated cells have the greatest increase of β(III)-Tubulin followed by the compound treatments that show similar expression levels that are higher than NT and -C cells. The higher expression of this marker validates the differentiation inducing activity of compounds 3, 4 and 10. **Figure 11C** investigates the expression of differentiation marker Growth Associated Protein 43 (GAP43) at 43 KDa. GAP43 expression was comparable in both the NT and -C groups, and cells treated with ATRA demonstrated an increase in the expression level of this differentiation marker. Cells treated with compound 3,4 and 10 have higher expression of GAP43 than -C treated cells. The increase of expression for compounds 3, 4, and 10 further supports the compounds as differentiation agents.

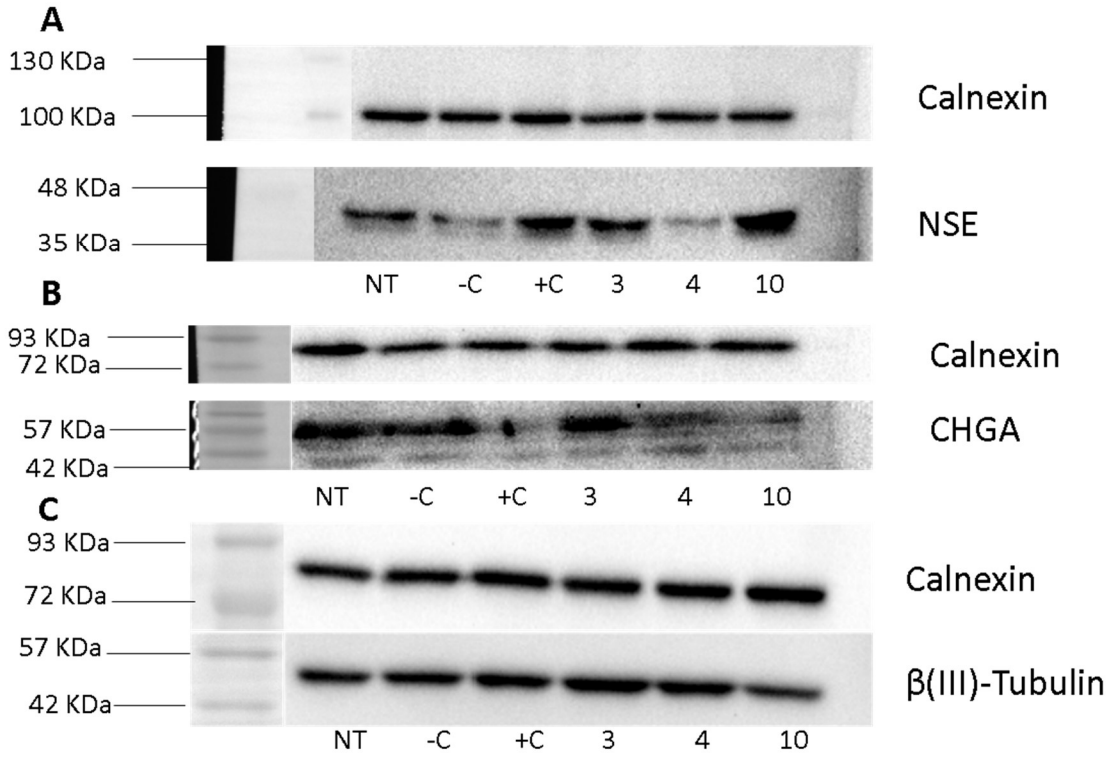

Figure 12. Expression of NSE, CHGA, and β(III)-tubulin in KELLY cells after treatment. A Shows the expression of Neuron Specific Enolase (~45 KDa) after 4-day treatment with compounds. NSE was loaded at a concentration of 20 ug per well. **B** Shows expression of CHGA (~48 KDa) after 4-day treatment with compounds. **C** Shows expression of β(III)-Tubulin (55 KDa) after 4-day treatment with compounds. Cell lysate was loaded at 5 µg. Treatments were added at a concentration of 12.5 µM and 5 µL for DMSO for negative control. Cell lysates were collected per treatment and stored at -20ºC. Calnexin (90 KDa) was used as a loading control and loaded at a concentration of 5 µg per well. NT= No Treatment, -C= DMSO (negative control), +C= ATRA (positive control), 3= Compound 3, 4= Compound 4, 10= Compound 10.

Expression of differentiation markers was also investigated in KELLY cells after 4 days of treatment and the results are shown in **Figure 12**. **Figure 12A** demonstrates the increase in expression of NSE for compounds 3 and 10, compared to NT, -C and compound 4. **Figure 12B** shows the expression of Chromogranin A, CHGA, which has been previously shown to be downregulated when differentiation is induced in neuroblastoma cells treated with retinoic acid [40]. For cells treated with ATRA, compounds 4 and 10, there is a decrease in expression of CHGA compared to negative

control treatments. Compound 3 unexpectedly did not cause a noticeable reduction in CHGA expression, despite being validated through NSE expression to induce differentiation as shown in **Figure 12A**. The decrease in expression of CHGA for cells treated with compound 4 and 10 further demonstrates that these compounds have differentiation-inducing activity. **Figure 12C** shows an increase in expression for β(III)-Tubulin in ATRA treated cells as well as compounds 3 and 4 treated cells, further validating 3 and 4 as differentiation agents through this marker.

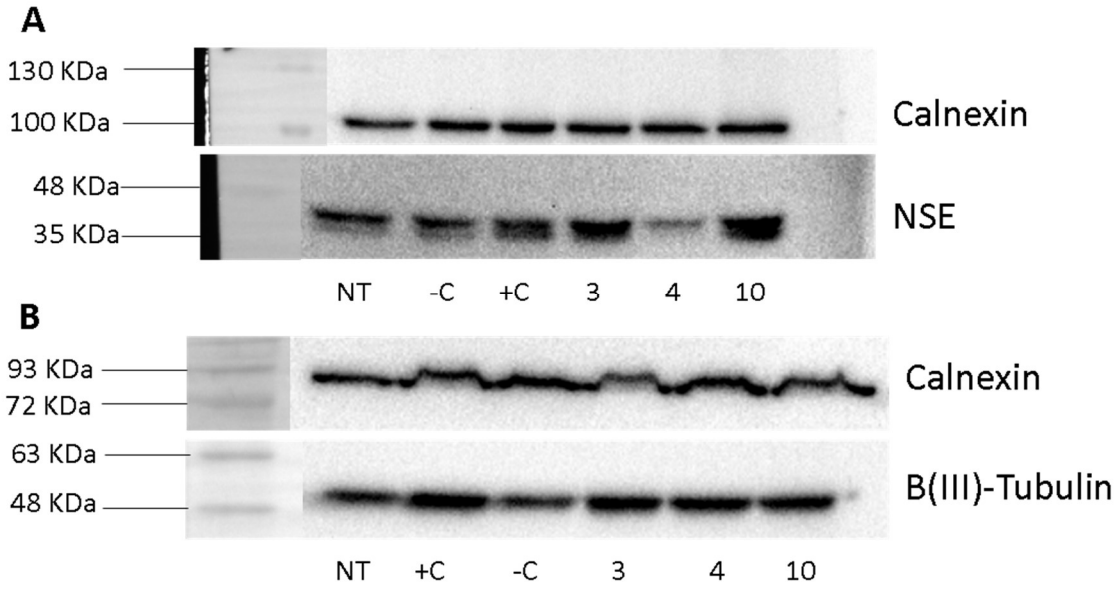

Figure 13. **Expression of NSE and β(III)-tubulin in CHLA-90 cells after treatment.** **A** Shows the expression of Neuron Specific Enolase (~45 KDa) after 4-day treatment with compounds. NSE was loaded at a concentration of 20 ug per well. **B** Shows expression of β(III)-Tubulin (55 KDa) after 4-day treatment with compounds. Cell lysate was loaded at 5 µg. Cells were treated with a concentration of 12.5 µM for each compound and 5 µL for DMSO for negative control. Cell lysates were collected per treatment and stored at -20ºC. Calnexin (90 KDa) was used as a loading control and loaded at a concentration of 5 µg per well. NT= No Treatment, -C= DMSO (negative control), +C= ATRA (positive control), 3= Compound 3, 4= Compound 4, 10= Compound 10.

Figure 13A depicts the expression of NSE in CHLA-90 cells after 4 day of treatments. The expression levels of NSE in ATRA and compounds 3 and 10 treated cells exceeds the expression levels in all other treatment groups. The expression of β(III)-tubulin is shown in **Figure 13B**, cells treated with ATRA and compounds 3, 4, and 10 show an increase in expression compared to NT and -C controls.

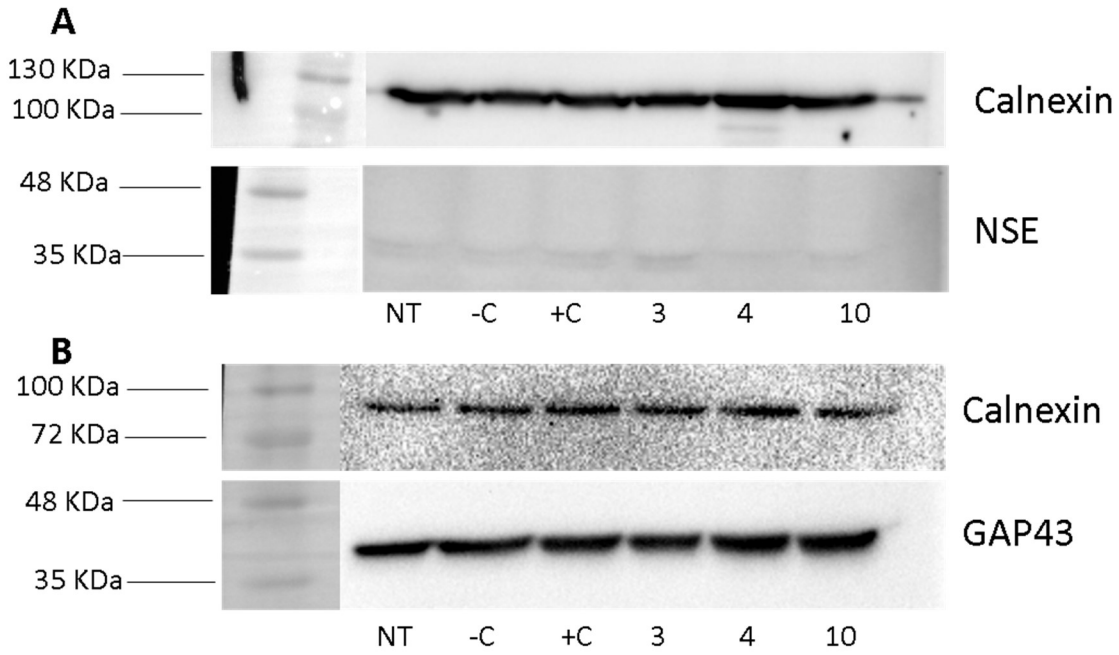

Figure 14. **Expression of NSE and GAP43 in SK-N-AS cells after treatment. A** Shows the expression of Neuron Specific Enolase (~45 KDa) after 4-day treatment with compounds. Cell lysate was loaded at a concentration of 20 µg per well. **B** Shows the expression of GAP43 (43 KDa) after 4-day treatment with compounds. Cell lysate was loaded at a concentration of 5 µg per well. Cells were treated with a concentration of 25 µM for each compound and 10 µL for DMSO for negative control. Cell lysates were collected per treatment and stored at -20ºC. Calnexin (90 KDa) was used as a loading control and loaded at a concentration of 5 µg per well. NT= No Treatment, -C= DMSO (negative control), +C= ATRA (positive control), 3= Compound 3, 4= Compound 4, 10= Compound 10.

Neuronal differentiation markers were also tested for in cell line SK-N-AS after four days of treatment as shown in **Figure 14**. **Figure 14A** is showing the expression of NSE, as seen there is a slight increase in expression for ATRA and compound 3 treated cells. In order to get a better idea if any other markers were being expressed, the expression of GAP43 was investigated. **Figure 14B** demonstrates that the expression of the differentiation marker is slightly increased in cells treated with compounds 4 and 10.

Table 2. Summary of Aim 1. This table summarizes the results of western blot analysis. In order to be validated through molecular differentiation markers, each cell line had to express high levels of NSE, β(III)-tubulin, and GAP-43; or a decrease in expression of CHGA.

Validated Differentiation Inducing Effect			
Cell Line	**Compound 3**	**Compound 4**	**Compound 10**
BE(2)-C	Y	Y	Y
KELLY	Y	Y	Y
CHLA-90	Y	N	Y
SK-N-AS	N	N	N

3.3 Effect of the three compounds on cell viability

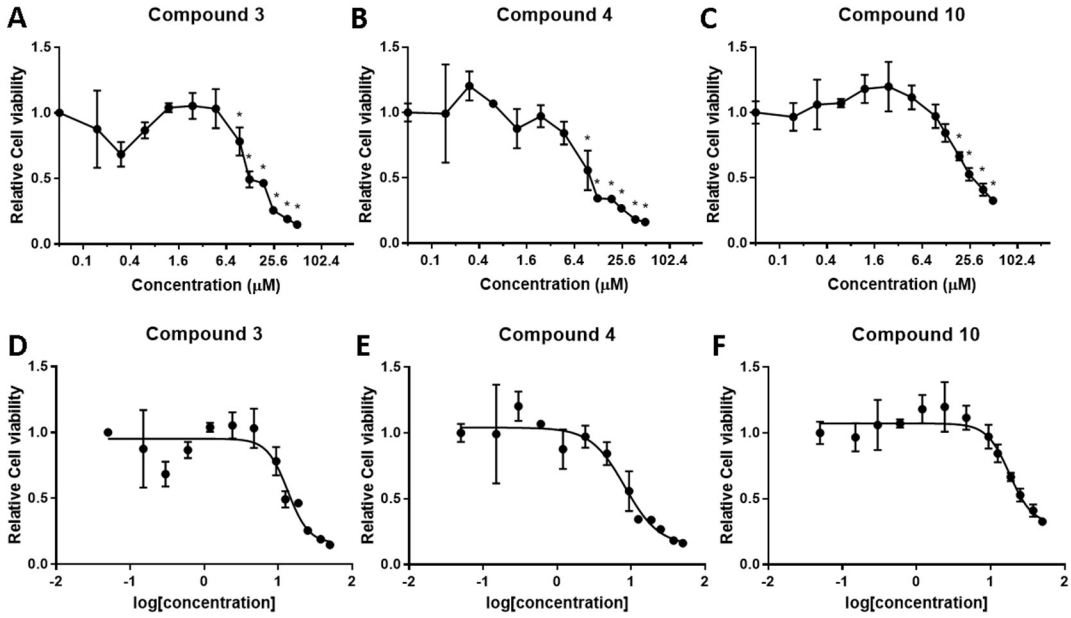

Figure 15. **BE(2)-C cell viability curves and IC_{50} graphs.** 1,000 BE(2)-C cells were plated in 96-well plates for each compound with concentration ranging from 0.15-50 μM. After 4 days, an MTT assay was performed. **A-B** MTT values were normalized to DMSO control and plotted to make dose-dependent curves. **D-F** IC_{50} graphs were modeled using Graphpad. The relative IC_{50} values are as follows: Compound 3 13.47 μM (R^2= 0.8695), Compound 4 8.22 μM (R^2=0.8875), and compound 10 is 18.00 μM (R^2=0.8965). *p<0.05

The goal of Aim 2 was to determine whether the compounds have a generic effect in reducing cell viability and inhibiting proliferation. **Figure 15** shows the dose-dependent effect on cell viability in BE(2)-C cells through dose-dependent cell viability plots (**A-C)** and IC_{50} graphs (**D-F)**. Compound 3 has a significant ($p < 0.05$) decrease in cell viability from 9.4 μM to 50 μM and a relative IC_{50} value of 13.47 μM with R^2= 0.8695, as demonstrated in **Figure 15A** and **Figure 15D**. As seen in **Figure 15B and 15E**, compound 4 also has a significant decrease in cell viability from 9.4 μM to 50 μM and the relative IC_{50} value is 8.22 μM with an R^2= 0.8875. **Figure 15C** and **15F** for

Compound 10 shows a significant decrease starting at 18.75 μM to 50 μM and the relative IC_{50} value is 18.00 μM with an R^2= 0.8965.

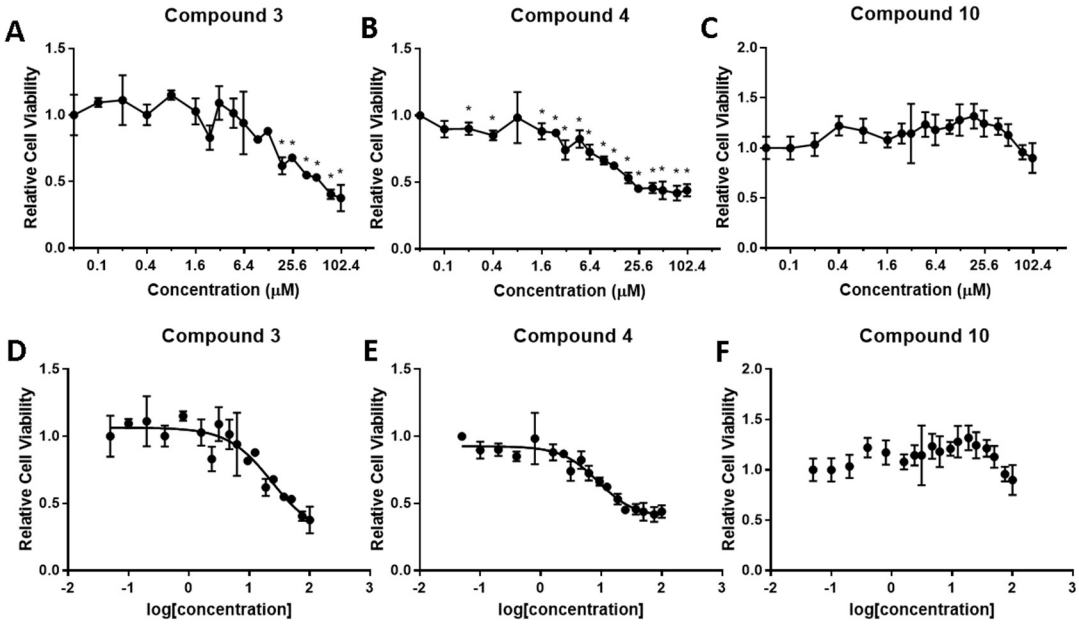

Figure 16. KELLY cell viability curves and IC_{50} graphs. 1,000 KELLY cells were plated in 96-well plates for each compound with concentration ranging from 0.10-100 μM. After 4 days, an MTT assay was performed. **A-C** MTT values were normalized to DMSO control and plotted to make dose dependent curves. **D-F** IC_{50} graphs were modeled using Graphpad. The relative IC_{50} values and R^2 are as follows: Compound 3 23.49 μM (R^2= 0.8267); Compound 4 8.89 μM (R^2=0.8946). *p<0.05

Figure 16A-C are the dose-dependent cell viability curves for KELLY cells and **Figure 16 D-F** are the IC_{50} graphs. Based on **Figure 16A** and **16D**, Compound 3 has a significant decrease in cell viability starting at 18.75 μM to 100 μM and its relative IC_{50} value is 23.49 μM with an R^2= 0.8267, implying a moderate fit to the non-linear curve. **Figure 16B** and **16E** show that compound 4 starts decreasing cell viability significantly at 0.2 μM to 100 μM and has a relative IC_{50} value of 8.89 μM with and R^2= 0.8946. **Figure 16F** for compound 10 cannot be fit into a non-linear curve to obtain an IC_{50} value,

the dose-dependent curve on **Figure 16C** demonstrates that there is no significant decrease in viability as concentration increases.

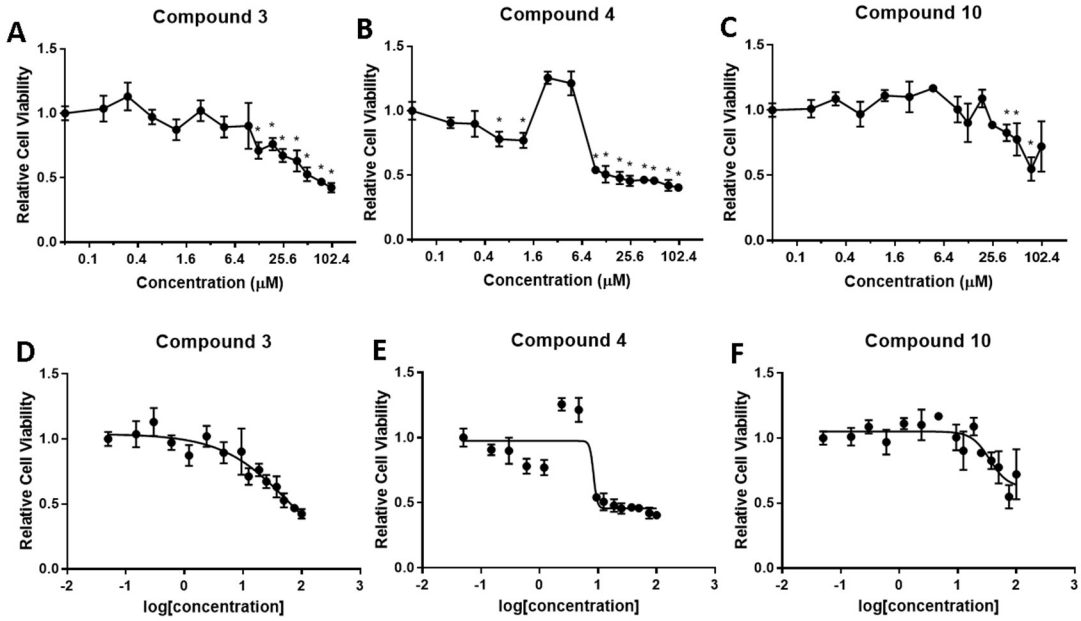

Figure 17. **CHLA-90 cell viability curves and IC_{50} graphs.** 3,000 CHLA-90 cells were plated in 96-well plates for each compound with concentration ranging from 0.15-100 μM. After 4 days, an MTT assay was performed. **A-B** MTT values were normalized to DMSO control and plotted to make dose-dependent curves. **D-F** IC_{50} graphs were modeled using Graphpad. The relative IC_{50} values and R^2 are as follows: Compound 3 60.33 μM (R^2= 0.8502); Compound 4 8.38 μM (R^2=0.786); Compound 10 35.16 μM (R^2=0.6496). *p<0.05

For CHLA-90, **Figure 17A** shows the significant decrease in cell viability for compound 3 from 12.5 μM to 100 μM, and **Figure 17D** lead to the relative IC_{50} of 60.33 μM with an R^2= 0.8502. **Figure 17B** and **17E** indicate a reduction in cell viability as a function of increasing concentration of compound 4, except for at 2.4 μM and 4.7 μM where there is an unexpected increase in cell survival, due to human error, the relative IC_{50} value is 8.38 μM with an R^2= 0.786. In **Figure 17C,** there is a siginificant decrease in cell viability in cells treated with compound 10, an effect that is observed at higher

concentrations compared to compounds 3 and 4. **Figure 17F** is the IC_{50} graph for compound 10, however the fit is poor according to the R^2 value of 0.6496, the IC_{50} concentration is 35.16 μM.

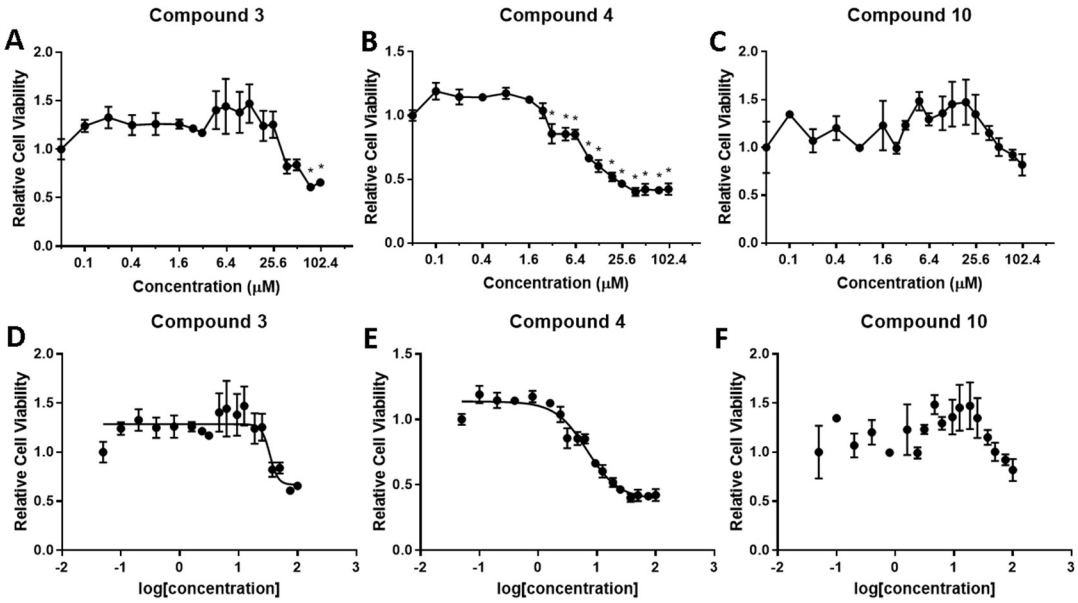

Figure 18. **SK-N-AS cell viability curves and IC_{50} graphs.** 1,000 SK-N-AS cells were plated in 96-well plates for each compound with concentration ranging from 0.10-100 μM. After 4 days, an MTT assay was performed. **A-B** MTT values were normalized to DMSO control and plotted to make dose-dependent curves. **D-F** IC_{50} graphs were modeled using Graphpad. The relative IC_{50} values and R^2 are as follows: Compound 3 33.89 μM (R^2= 0.692); Compound 4 6.788 μM (R^2=0.9554). *p<0.05

The same investigation into the effects of the compounds on cell viability was performed in SK-N-AS cells. **Figure 18A** and **18D** demonstrate that SK-N-AS cell viability does not significantly decrese until higher concentrations of compound 3 are used. The relative IC_{50} value obtained from **18D** is 33.89 μM, however the correlation is poor as indicated by the R^2 of 0.692. Compound 4 values had a great fit with an R^2 of 0.9554 and therefore a more accurate IC_{50} value of 6.788 μM is seen in **Figure 18E**. The dose-dependent cell viability plot**, Figure 18B**, shows a significant decrease in cell

viability starting at 3.125 µM to 100 µM. The dose-dependent cell viability plot for compound 10, shown in **Figure 18C**, had no significant decrease in cell viability despite the appearance of a slight decrease. **Figure 18F**, the modeling could not be performed on the values therefore no IC_{50} value was obtained.

Table 3. Relative IC_{50} values. This table summarizes the results obtained for the modeling of the cell viability assay per cell line. For compound 10, results for cell lines KELLY and SK-N-AS were not able to be modeled.

Relative IC_{50} Values			
Cell Line	**Compound 3 (µM)**	**Compound 4 (µM)**	**Compound 10 (µM)**
BE(2)-C	13.47	8.220	18.00
KELLY	23.49	8.890	N/A
CHLA-90	60.33	8.380	35.16
SK-N-AS	33.89	6.788	N/A

3.4 Effect of the three compounds on colony formation

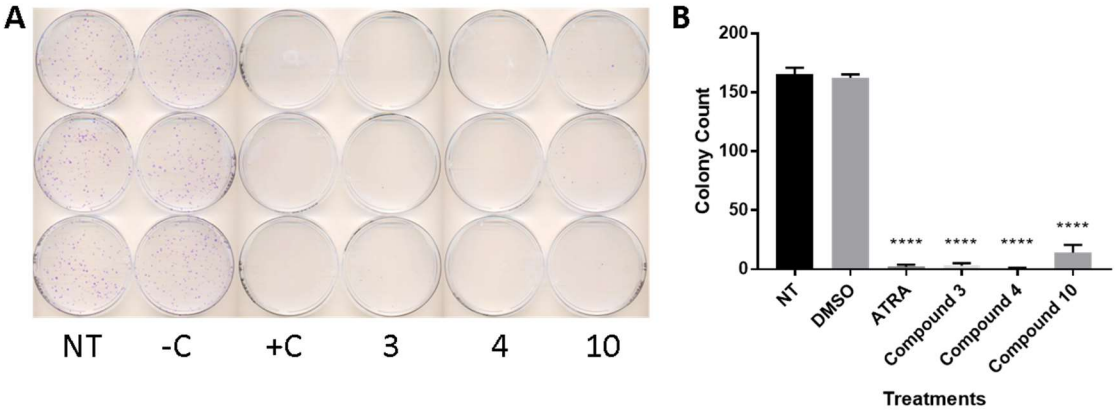

Figure 19. BE(2)-C colony formation assay. A 1,000 BE(2)-C cells were plated in 100 mm dishes and incubated for 12 days. Colonies were fixed and stained using Crystal Violet. **B** Cell count was performed using ImageJ and statistical analysis was performed using Graphpad. ****, $p < 0.0001$.

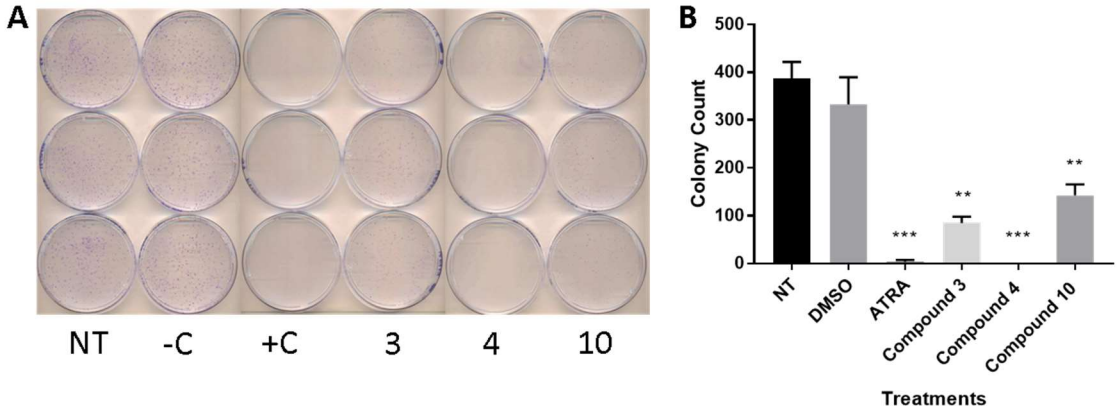

Figure 20. KELLY colony formation assay. A 2,000 Kelly cells were plated in 100 mm dishes and incubated for 12 days. Colonies were fixed and stained using Crystal Violet. **B** Cell Count was performed using ImageJ and statistical analysis was performed using Graphpad.***p<0.001, **p<0.01.

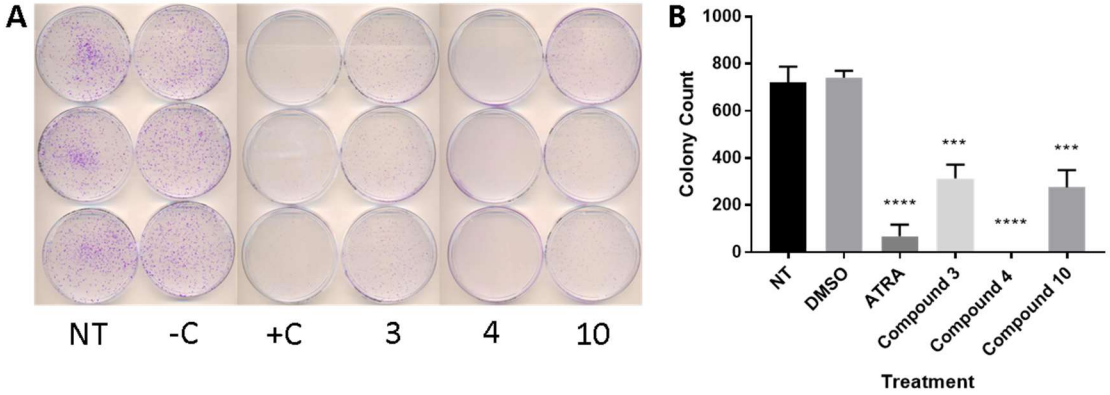

Figure 21. CHLA-90 colony formation assay. A 2,500 CHLA-90 cells were plated in 100 mm dishes and incubated for 12 days. Colonies were fixed and stained using Crystal Violet. **B** Cell Count was performed using ImageJ and statistical analysis was performed using Graphpad.****p<0.0001, ***p<0.001.

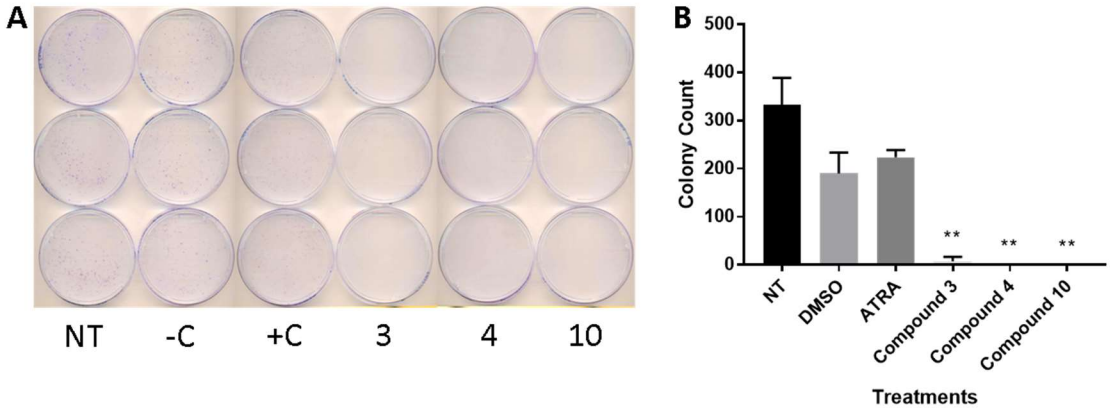

Figure 22. SK-N-AS colony formation assay. A 2,000 SK-N-AS cells were plated in 100 mm dishes and incubated for 12 days. Colonies were fixed and stained using Crystal Violet. **B** Cell Count was performed using ImageJ and statistical analysis was performed using Graphpad.**$p<0.01$.

Aside from effects on cell viability, the compounds were also investigated for their effect on cell proliferation. As seen in **Figure 19**, ATRA and compound treatments inhibit proliferation significantly in BE(2)-C cells. In accordance with previous experiments, compound 10-treated plates had more colonies present than compounds 3, 4 and ATRA plates. **Figure 20** investigates the effects of cell proliferation in KELLY cells. Results indicate that ATRA and compound treatments do significantly inhibit proliferation in KELLY cells with ATRA and compound 4 depicting the greatest inhibition. ATRA and compound treatment also inhibit the proliferation capabilities in CHLA-90 cells as seen in **Figure 21**. However, the effect of compounds 3 and 10 is significantly lower than compound 4. For SK-N-AS cells, shown in **Figure 22**, there was a decrease in colonies between the negative control and no treatment control, which had not been seen previously. ATRA treated cells were not inhibited compared to DMSO, however compound treatments did have a significant inhibition effect when compared ot DMSO plates.

3.5 Effect of the three compounds on cell apoptosis in neuroblastoma cells

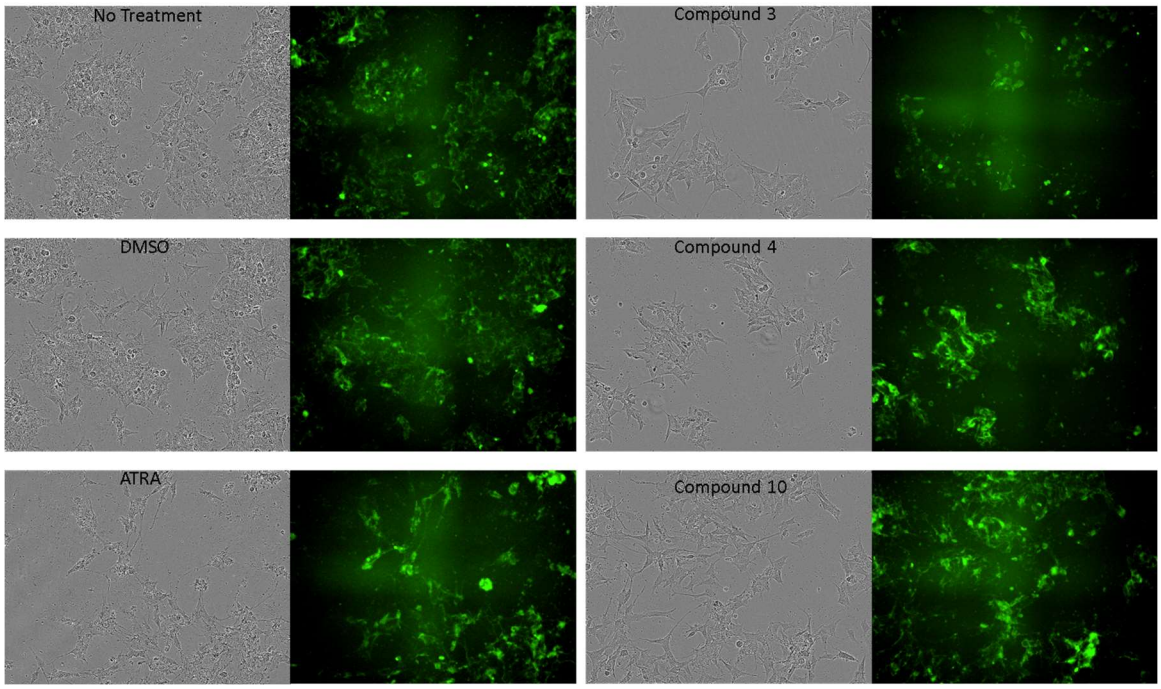

Figure 23. Activated Caspase3/7 apoptosis assay in BE(2)-C cells. 1,500 cells per well were plated in a 96-well plate. Cells were treated with 12.5 µM for each compound and 2 µL of DMSO for negative control wells. Cells were incubated for 4 days. After 4 days, a solution containing CellEvent™ Caspase 3/7 Green Detection Reagent and 10%EFBS PBS was added to the wells. Plate was imaged after 30 minutes of incubation using Incucyte.

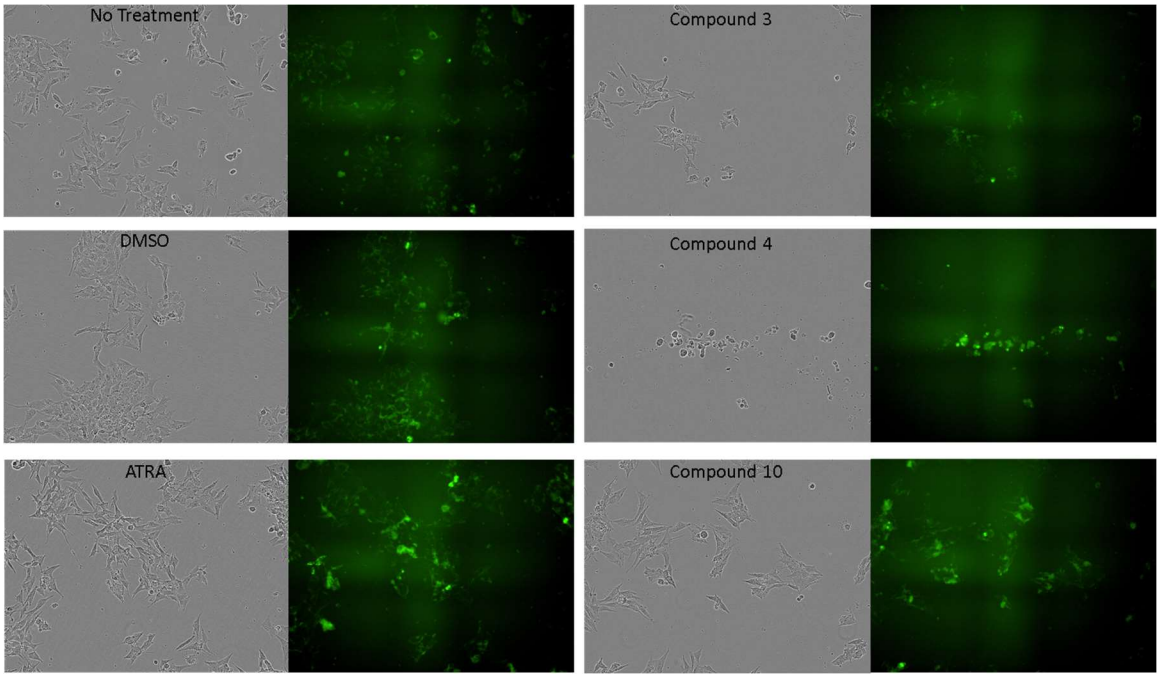

Figure 24. Activated Caspase3/7 apoptosis assay in KELLY cells. 1,500 cells per well were plated in a 96-well plate. Cells were treated with 12.5 µM for each compound and 2 µL of DMSO for negative control wells. Cells were incubated for 4 days. After 4 days, a solution containing CellEvent™ Caspase 3/7 Green Detection Reagent and 10%EFBS PBS was added to the wells. Plate was imaged after 30 minutes using Incucyte.

One of the goals of Aim 3 was to determine the mechanism of cell death induced by the compounds. **Figure 23** indicates the reults of an activated Caspase 3/7 assay in BE(2)-C cells. Cells treated with ATRA, compound 4 and compound 10 show more fluoresence than cells untreated or treated with DMSO. These indicate that cells treated with ATRA and compounds 4 and 10 have more cells activating Caspase 3/7 and inducing apoptosis comparing to control. However, compound 3 has no such effect. In **Figure 24**, the same assay was performed in KELLY cells. Similar to BE(2)-C cells, ATRA and compounds 4 and 10 have more cells fluorescing than DMSO, compound 3, and untreated cells. This suggests that more cells under treatments of compounds 4 and 10 are activating Caspase 3/7, therefore inducing apoptosis.

3.6 Effect of the three compounds on cell cycle distribution

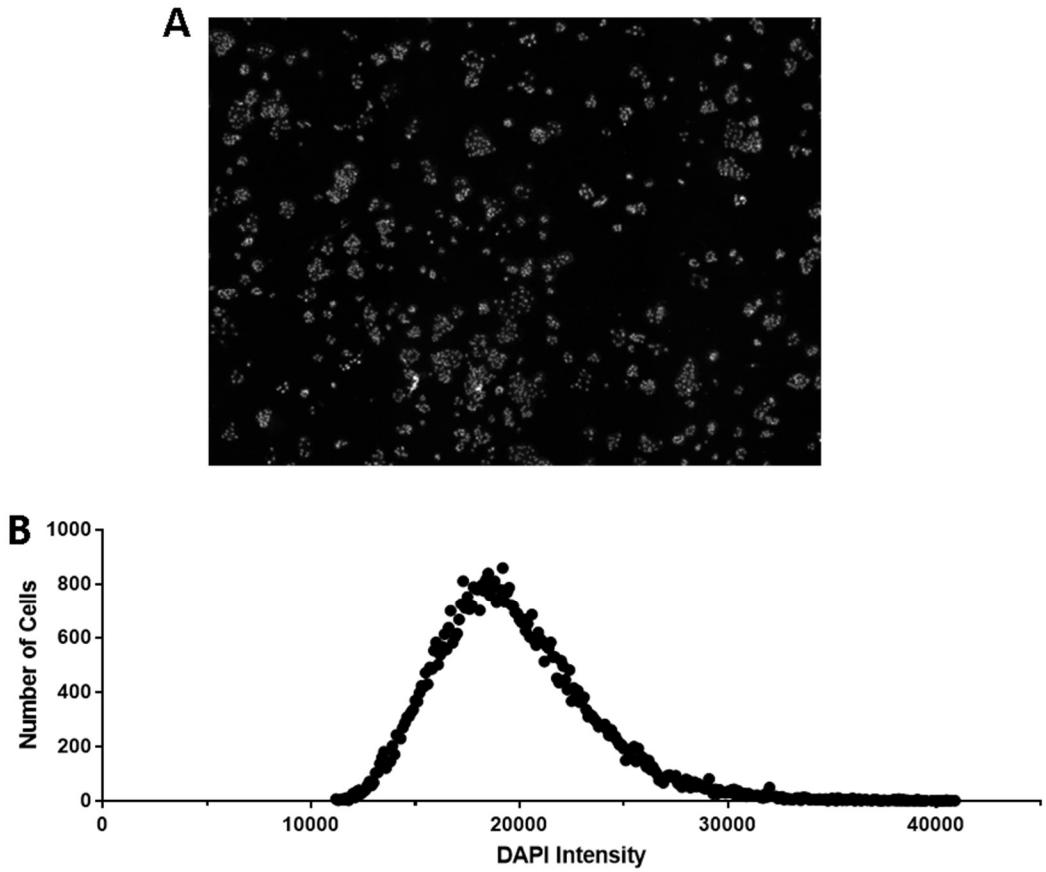

Figure 25. Cell cycle analysis using DAPI staining in A549 cells. 120,000 A549 cells were grown in 60 mm dishes until confluency was at its maximum. Cells were then fixed and stained with DAPI. **A** A549 DAPI stained cells were imaged using the Lionheart FX at 20X. **B** DAPI intensities and cell count were obtained through the Lionheart FX software. Cells per intensity was plotted to produce graph.

To asses whether the DAPI staining approach can be used to determine cell cycle distribution, the lung cancer cell line A549 was used to provide a standardized analysis of producing a cell cycle histogram based on DAPI staining. **Figure 25A** shows a picture of the cells taken from 20X using a Lionheart imagr station, and zoomed in for analyzing. As seen, the clusters of cells are hard to distinguish at this magnification. **Figure 25B** is a plot of the DAPI intentisties recorded for every cell picked up by the Lionheart FX software. There is a clear peak at around 20,000 units, however no other peak is visible in

order to distingush different phases of the cell cycle. These results suggest that cell cylce histogram can not be obtained using the current settings in the Lionheart FX system. Future explorations are needed.

3.7 Investigation into compound treatment induced cell senescence

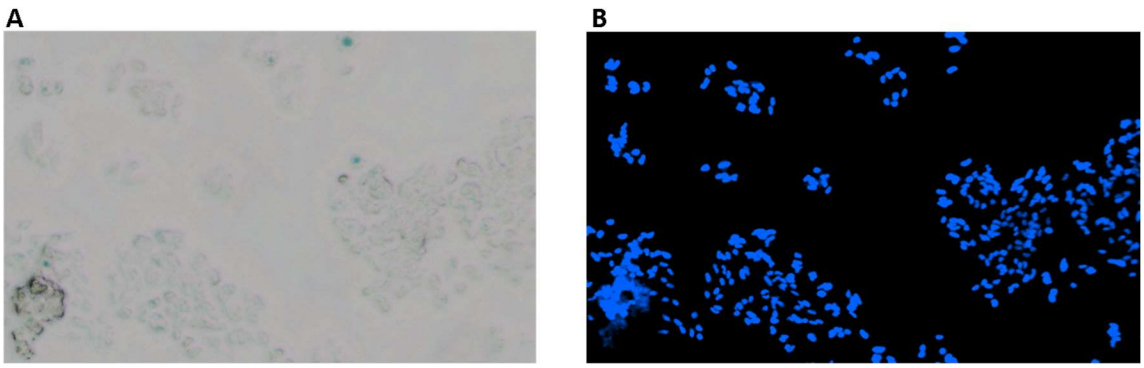

Figure 26. Senescence-associated beta-galactosidase staining in KELLY cells. 200,000 KELLY cells were grown in 60 mm dishes for 6 days with 12.5 µM of ATRA. Cells were then fixed and stained with fresh staining solution and DAPI. **A** KELLY stained cells were imaged using the color brightfield in the Lionheart FX at 4X. **B** DAPI stained KELLY cells imaged at 4X.

A senescence-associated β-galactosidase assay was performed to investigate the effect of ATRA on KELLY cells. **Figure 26A** shows the color brightfield image of KELLY cells, where cells expressing blue coloration were cells with SA-β-gal activity and therefore cells in a scenescnet state. **Figure 26B** is an image showing DAPI staining, which was used to identify which cells were expressing the blue color. This is a pilot sutdy without any negative control treatments being used. Future work is clearly needed to further determine whether this approach is sensitive and specific enought to determine the effect of compound treatments on cell senescence.

4. DISCUSSION

To begin analyzing these results and establishing whether compounds 3, 4, and 10 have generic differentiation-inducing activity in neuroblastoma cells with different genetic backgrounds, more information about cell lines used in this study is needed. **Table 2** lists the characteristics of each cell line used and whether they show responsiveness to RA and the subtype they have been charactarized as. The subtype is important to know in order to explain the responses obtained for each cell line. BE(2)-C has been documented to be responsive to retanoic acids. Cells that are treated tend to stop proliferating, and resume the differentiation process. This includes a change in morphology, where neurite processes are visualized and this change in morphology is referred to as the neuronal phenotype.[41-43] While background on KELLY cells is minimal, they have been shown to be responsive to RA and differentiate into the neuronal phenotype, with neurite processes also manifesting during differentiation.[44] CHLA-90 cells, which is an anti-cancer drug resistant cell line, have also been characterized as being partially responsive to RA through inhibition of proliferation.[45-47] RA has also been shown to partially inhibit proliferation for SK-N-AS, but does not differentiate cells, therefore they remain in their S-type morphology of being flat and round without processes.[48]

Table 4. Neuroblastoma cell line characteristics. This lists the patient information and site from which the cell line was derived. It also says whether or not the cell line is responsive to RA according to the literature. It also lists whether the cell lines is charactarized as a Neuroblastic-type, Intermediate-type, or Substrate-adherent-type.

Cell Line	Sex	Age	Stage	Site	Responsive to RA	Subtype
BE(2)-C	M	2 yrs	4	Bone Marrow	yes	I-type
KELLY	unk	unk	unk	Brain	partially	N-type
CHLA-90	M	8.5 yrs	4	Bone Marrow	yes	N-type
SK-N-AS	F	6 yrs	unk	Bone Marrow	no	S-type

Neurite porjections have been demonstrated to be a strong indicator of differentiation in some neuroblastoma cell lines, as it resembles a mature neuron ready to form a functional network.[49, 50] Therefore, as part of Aim 1, the quantification of neurite length at ranging concentrations of compounds was investigated in this study and the results are shown in **Figures 7-10**.

As seen for BE(2)-C cells in **Figure 7**, the neurite projections increased in length as concentration increased to 50 μM for all three compounds. Previous studies have linked the increase of neurite projections to differentiated cells.[51, 52] BE(2)-C cells, an I-type cell line, have been documented as being able to differentiate between neuronal type cells and non-neuronal cells.[42] This means that the neurite outgrowth assay can be used as a great indicator for initial differentiation in BE(2)-C cells, understanding that there are some BE(2)-C cells that are differentiated into the non-neuronal type.[41, 42] KELLY cells have been documented as being able to grow neurites[53], but whether neurite length increases in response to retinoids has not been established for this cell line. The cell line is classified as being only partially responsive with respect to differentiation

when treated with RA.[44, 54] **Figure 8** provides insight into whether the compounds induce neurite outgrowth in KELLY cells. Compounds 3, 4, and 10 induce a significant increase in neurites at lower concentrations, and seem to be more sensitive to compound treatment as neurite lengths decreased dramatically at higher concentrations. CHLA-90 cells grow normally with long neurite projections without any treatment. **Figure 9** fails to demonstrate an increase upon compound treatment, and eventually for all three compounds neurite lengths decrease. The large error bars obtained can be explained by the variance in neurite lengths already observed in the cell line without treatment. The neurite outgrowth assay was also performed on SK-N-AS cells, **Figure 10** shows that neurite outgrowth cannot be quantified. This is consistent with S-type cells that are flat with a large surrounding extracellular matrix and differentiate into non-neuronal type of cells which show the same morphology.[42, 43] It has also been shonw that RA does not induce a morphological change in SK-N-AS cells.[48]

To determine and better support whether differentiation is being induced by compound treatments, the expression of differentiation markers was investigated in all four cell lines. In **Figure 11A**, NSE is expressed in higher amounts in cells that were treated with ATRA and compounds 3 and 10 in BE(2)-C. However compound 4 treated cells had minimal NSE expression, therefore, the differentiation-inducing effect of compound 4 was not considered as validated through this differentiation marker. **Figure 12A** shows a similar increase in expression of NSE in KELLY cells, again validating compounds 3 and 10 as differentiation markers. There is also a slight increase in expression of NSE for CHLA-90 cells as seen in **Figure 13A**. Interestingly, in **Figure 14A** for SK-N-AS cells, there is an increase in expression for only ATRA treated cells

and compound 3 treated cells. NSE has been deemed a neuron specific glycolytic isozyme and is highly expressed in differentiated neurons and its expression is increased during the maturation process of neurons.[55, 56] NSE levels in cultured cells tend to be lower, although the difference between tumor expression and cell line expression is still unclear, however higher expression of NSE in cell lines has been linked to neuronal differentiation in neuroblastoma.[57] [56, 58] Therefore compound 3 is validated in all four cell lines through NSE expression and compound 10 is validated in three out of the four cell lines.

BE(2)-C cells treated with ATRA and the three compounds also express β(III)-tubulin at higher amounts than the no treatment cells and DMSO-treated cells, as seen in **Figure 11B**. The higher expression of this protein can be related to differentiation as it has been previoulsy noted to increase in some cell lines after the treatment with RA and other agents.[35, 59] β(III)-tubulin is a microtubule isotype that is present in small quanities and is mostly seen in neurons and testis.[60] During neuroblastoma differentiation in SK-N-SH, β(III)-Tubulin is distributed throughout the cell body and neurites helping to support the projections.[61] PC-12 cells are a rat clonal cell line used as the mammilian cell model in order to understand the distribution and expression of β-tubulin after differentiation with nerve growth factor (NGF). The accumulation of β(III)-tubulin in neurite outgrowth alone with 5 other isotypes has been seen in PC-12, therefore setting precendent for β(III)-tubulin as a differentiation marker.[62] The increase of β(III)-tubulin expression for ATRA and compound treatment in BE(2)-C cells is therefore expected as ATRA and the three compounds induced growth of neurite projections and therefore required more β(III)-tubulin. As shown in **Figure 12C** for KELLY cells there is an increase in β(III)-

tubulin expression observed for ATRA and compound 3 and 4 treatments. Unexpectedly, treatment with compound 10 did not increase β(III)-tubulin expression. In CHLA-90 cells treated with ATRA and compounds 3, 4, and 10 there was also an increase in expression like BE(2)-C cells as shown by **Figure 13B**. Although there is no increase in neurite lengths, the increase in β(III)-tubulin can be explained by increased neurite projections as cells undergo differentiation into the neuronal type.[42, 61, 62]

GAP-43 has been established as a neuronal marker known to play a role in growth cones of neurons, and is expressed at high amounts during neuron development as well as during regeneration and restoring of plasticity in regenerated and repaired cells.[63, 64] GAP-43 has been implicated as assisting and potentiating neurite outgrowith in neuronal cells[65], and in neuroblastoma cells after differentiation with RA.[35, 66, 67] Since there is an increase in neurites with compound treatements and ATRA, treatment is expected to increase GAP-43 expression. As expected, GAP- 43 expression is increased upon ATRA and compound treatments for BE(2)-C cells, as shown in **Figure 11C**. There was also an increase in expression of this protein in cells treated with compounds 4 and 10 in SK-N-AS cells as seen in **Figure 14B**. S-type cells do not express neurite outgrowth when introduced to differentiation agents. Through the characterization of neuroblastoma subtypes, it was found that S-type undifferentiated cells express a basal level of GAP43.[68] An increase in expression of GAP-43 in the epithelial neuroblastoma subclone cell line, SH-EP, was observed after differenitation with 12-O-tetradecanoyl-phorbol-13-acetate (TPA).[69] The overall function of GAP-43 has not been elucidated, but evidence of the expression of GAP-43 in non-neuronal cells has lead to the hypothesis that this protein has a function in regulation of cell shape and rearrangement. Therefore the increase in

expression of GAP-43 in SK-N-AS cells treated with compounds 4 and 10 can be explained as the accumulation of the protein during differentiation due to potential rearrangemnt and cell surface reactions and is related more to the role of GAP-43 in neuroplasticity than neurite outgrowth.[64, 70, 71]

CHGA is a storage protein for neuroendocrine cells, it also has a role in regulating change in phenotype, proliferation and differentiation of neuroblastoma cells and the depletion of CHGA has been linked to decreased proliferation in neuroblastoma cells.[40, 72] CHGA has been shown to be negatively regulated by RA, however it is upregulated whenever cells are treated with cAMP, due to RA and cAMP inducing differentiation in neuroblastoma through different pathways.[40] **Figure 12B** shows the expression of CHGA in KELLY cells, with ATRA and compounds 4 and 10 decreasing expression of CHGA and compound 3 expressing similar amounts to controls. These results therefore suggest that ATRA and compounds 4 and 10 are acting on the same differentitation pathway, while compound 3 is acting on a separate pathway that does not upregulate CHGA. The expression of differentiation markers by each cell line is expected. The cells are of different subtypes, and depending on what agent is inducing differentiation dictates which differnetiaiton pathway they will adopt. For example, N-type and I-type cells tend to differentiate to neuronal type cells when induced by RA.[42, 43] They can also be differentiated into non-neuronal type, which resemble the S-type morphoplogy, by Bromodeoxyuridine. S-types are typically differentiated into non-neuronal types, which resemble ephithelial cells and does not include a morphological change but it does include change in genotype.[34, 43, 68]

Aim 2 was focused on investigating whether the compounds inhibit proliferation and induce cell death. During embryonal development cell proliferation is regulated. However when there are mutations and disruptions through mutations and or other alterations, proliferation gets disregulated. This is commonly seen in tumors and therefore there are drugs that are meant to target proteins in pathways involved in cell proliferation.[73] RA inhibits proliferation but the extend of supression is dependent on the cell line.[32, 33, 73, 74]. RA inhibits proliferation *in vitro* by maturation, and it only partially induces a late form of apoptosis after days of treatment with clinincally relevant concentrations.[75, 76] Whereas there are other drugs that inhibit growth by inducing cell death through apoptosis and necrosis and not inducing differentiation, such as N-(4-Hydroxyphenyl)retinamide (4-HRP), or fenretinide.[75-77] Compound 3 seems to induce cell death at lower concentrations as compared to compound 10. However the dose-dependent cell viability curves of compound 3 , as shown in **Figures 15-18A**, are flatter than compound 4 curves, meaning it takes a higher concncetration of compound 3 to induce cell death. IC_{50} values for compound 3 range from 13.47-60.33 μM. The fits of compound 3 IC_{50} curves shown in **Figures 15-18D** are relatively low indicating that these values have greater variences. Compound 3 also significantly decreased colony formation in all four cell lines compared to DMSO control, however colonies were still present after the 12 day incubation. Compound 3 resembles RA in that it seems that inducing differentiation is the main way to inhibit proliferation rather than inducing cell death immediately.

Compound 4 induces death at lower concentrations in 3 out of the 4 cell lines as demonstrated by **Figures 16-18B**. The IC_{50} values for compound 4 are also the lowest out

of the three compounds ranging from 6.788-8.89 μM with relatively high R^2 values. Through **Figures 19-22**, it is observed that compound 4 significantly inhibits colony formation growth, with all plates exhibiting no colonies after the 12 days of incubation. Compound 4 resembles 4-HRP, in that treatment induces cell death rather than differentiation. Our results suggest that the main mechanism of inhibiting proliferation by this compound is through directly inducing cell death. Compound 10 induced cell death in BE(2)-C cells and CHLA-90 cells in a dose dependent manner, as shown in **Figures 15C and 17C**. The concentrations at which cell viability decrease significantly were higher than the other two compounds. The IC_{50} values for compound 10 were only able to be obtained from BE(2)-C cells (**Figure 15F)** and CHLA-90 cells (**Figure 17F**), and were 18.00 and 35.16 μM with a relatively low fit for the CHLA-90 IC_{50} curve (**Figure 17F**). For KELLY and SK-N-AS cells, compound 10 decreased cell viability at higher concentrations, however not significantly. In **Figures 19-22**, depicting the colony formation assays for the four cell lines, compound 10 significantly decreased the number of colonies present after the 12 days of incubation. The number of colonies for compound 10 in cell lines BE(2)-C and KELLY were greater than the number of colonies found for other compounds, demonstrating that compound 10 is less potent in these two cell lines than compounds 3 and 4. Intererstingly, while compound 10 did not significantly decrease cell viability for KELLY cells and SK-N-AS cells, it did inhibit proliferation as shown by **Figure 20** and **Figure 22**, respectively. These results suggest that compound 10, similar to RA, induces differentiation but does not induce cell death until higher concentrations or after days of treatment. An important limitation to understand is the modeling system used to identify the relative IC_{50} values. The values are not absolute

IC_{50} values as this value requires modeling of a sigmoidal curve, instead these are relative values predicted from the absorbance data.

The goal of Aim 3 was to investigate the mechanism by which the compounds induce cell death in the four cell lines studied. Using CellEvent™ Caspase-3/7 Green Detection Reagent, an apoptosis assay was set up. According to the ThermoFisher manual, the reagent works by consisting of a dye with four amino acid peptide that when cleaved by the activation of Caspase 3 or Caspase 7, will allow the dye to bind to DNA and fluoresce. The results for the BE(2)-C and KELLY cell lines are shown in **Figures 23** and **24**. The assay needs to be modified to subtract the background fluorescence in order to be able to quantify the amount of cells that are fluorescing. Using the phase contrast picture and the green fluorescence picture, it is clear that cells that are treated with ATRA as well as compounds 4 and 10 have more cells fluorescing than compound 3 treated cells. Therefore, it can be speculated that compounds 4 and 10 are inducing apoptosis after 4 days of treatment, while compound 3 treatment lead to cell death through another mechanism. However, there were limitations to this assay due to fewer cells being alive at the end of the four day treatment for compounds 3 and 4. The assay was also performed with two concentrations, 12.5 μM and 25 μM, but there were two few cells to be detectable with 25 μM treatment. The background fluorescense interefered with quantification performed with the images, and it was concluded that the Incucyte was not sensitive enough to quantify apoptosis using this approach.

A cell cycle analysis was attempted using a lung cancer cell line, A549, which had been previously identified as a reference cell line for performing cell cycle analysis. The cell line was prepared and imaged as stated in the methods. **Figure 25A** is an image

taken at 20X, in order to determine whether using this magnification would allow for proper counting and measuring of cell cycle by the software available in the Lioneart FX. The results indicated that many of the clusters of cells would be counted as one cell and when attempting to separate the cells through changes in parameters, a large amount of cells had to be excluded from the quantification. Unfortunately, the histogram attempted in **Figure 25B** demonstrated that the methodology was not sensitive enough to distinguish cell cycle phases. There have been studies that use DAPI staining as a method to do cell cycle analysis, but most use flow cytometry or algorithims that help deconvolute and model the different phases using confocal microscopy.[36, 78, 79]

Although not part of the aims, cell senescence was investigated through a senescence-associated β-gal assay. Senescence is defined as the irreversable arrest of cell growth after a definite amount of times of replication, and has been identified as a mechanism for tumor suppression.[80, 81] The detection of the activity of β-gal at a pH of 6.0 has been described as a marker for senescence since quiascent or terminally differentiated cells do not express this activity under the same condition.[80] The activity of β-gal is observed through the addition of X-gal, which gets cleaved by the enzyme producing a dense blue product.[81] RA has been shown to induce G1 arrest through neuronal differentiation and senescence, depending on cell line characteristics such as subtypes.[31] S-type cells are more prone to entering senescence than N-type cells in neuroblastoma, although it depends strictly on the cell line itself.[31, 82] This assay was performed in KELLY cells after treatment with 12.5 μM ATRA, and the results show that there are senescent cells present after 6 days of treatment. As **Figure 26B** depicts, it is hard to distinguish cells that are clustered together at 4X, and the Lionheart FX software

was not able to distinguish clustered cells in order to perform cell counts. Another limitation of the assay was that the color brighfield mode was only available at 20X, and the outlines of cells were tougher to distinguish and focus on at this maginifcation.

In conclusion, compound 3 is validated as having differentiation-inducing activity in three cell lines as demonstrated in **Table 2**. **Table 3** demonstrates compound treatment induces cell death and results for colony formation show that it inhibits proliferation significantly in all cell lines studied. However, there should be more investigation over the mechanism by which compound treatment induces cell death as it seems to not induce apoptosis in BE(2)-C or KELLY cells. **Table 2** demonstrates that compound 10 is validated in three cell lines as well. Nevertheless, compound 10 does not appear to be inhibiting proliferation through the induction of cell death as demonstrated in **Table 3**. Instead it seems to be acting only by maturing neuroblastoma cells, while possibly inducing late apoptosis events only at higher concentrations. It could also be that it takes longer time for the apoptosis pathway to be activated. Therefore more investigation into the cell cycle distribution should be explored, along with investigating apoptosis for longer time periods of treatment with the compound. Compound 4 is demonstrated to increase neurite lengths in BE(2)-C cells and KELLY cells, while increasing expression of GAP43 and β(III)-tubulin within the four cell lines. It could be that the compound is activating a stress response in the cells that allows for the increase in neurite projections which have been documented previously.[83, 84] While the differentiation-inducing activity of compound 4 is only validated in two cell lines (**Table 2**), the induction of cell death by this compound has been observed for the four cell lines in this study as demonstrated in

Table 3. It is possible that compound 4 mainly acts as a neuroblastoma apoptosis inducer, like 4-HRP, rather than a differentiation agent.

Future studies should move forward with compound 3 and should investigate the effect of the compound on the cell cycle distribution using a more sensitive approach such as flow cytometry, accompanied by western blot analysis of cell cycle regulators. Potential markers for apoptosis based on propidium iodide staining of DNA, DAPI for DNA fragmentation, or analysis of annexin V binding.[85] Furthermore, other mechanisms of programed cell death, such as programmed necrosis or autophagy, should be investigated in order to get a better idea of potential pathways activated by the compound.[86-88] Lastly, in order to investigate whether the compound is inducing senescence in the multiple cell lines, flow cytometry or confocal microscopy should be used in order to quantify SA β-gal results and obtain comparable results as well as flow cytometry for Senescence Associated Heterochromatin Foci (SAFH).[80, 81, 89]

REFERENCES

1. Brodeur, G. M., Neuroblastoma: biological insights into a clinical enigma. *Nature Reviews Cancer* **2003,** *3* (3), 203.

2. Medrano, G.; Du, L.; Betancourt, T.; Lewis, K., *Determining the role of ATP6V0E1 of the vacuolar-ATPase in regulating neuroblastoma cell survival and differentiation*. 2018.

3. Louis, C. U.; Shohet, J. M., Neuroblastoma: molecular pathogenesis and therapy. *Annu Rev Med* **2015,** *66*, 49-63.

4. Park, J. R.; Eggert, A.; Caron, H., Neuroblastoma: biology, prognosis, and treatment. *Hematol Oncol Clin North Am* **2010,** *24* (1), 65-86.

5. Davidoff, A. M., Neuroblastoma. *Semin Pediatr Surg* **2012,** *21* (1), 2-14.

6. Walton, J. D.; Kattan, D. R.; Thomas, S. K.; Spengler, B. A.; Guo, H. F.; Biedler, J. L.; Cheung, N. K.; Ross, R. A., Characteristics of stem cells from human neuroblastoma cell lines and in tumors. *Neoplasia* **2004,** *6* (6), 838-45.

7. Takahashi, Y.; Sipp, D.; Enomoto, H., Tissue interactions in neural crest cell development and disease. *Science* **2013,** *341* (6148), 860-3.

8. Huber, K., The sympathoadrenal cell lineage: specification, diversification, and new perspectives. *Dev Biol* **2006,** *298* (2), 335-43.

9. De Zio, D.; Giunta, L.; Corvaro, M.; Ferraro, E.; Cecconi, F., Expanding roles of programmed cell death in mammalian neurodevelopment. *Semin Cell Dev Biol* **2005,** *16* (2), 281-94.

10. Van Arendonk, K. J.; Chung, D. H., Neuroblastoma: Tumor Biology and Its Implications for Staging and Treatment. **2019,** *6* (1), 12.

11. Nowak, D.; Stewart, D.; Koeffler, H. P., Differentiation therapy of leukemia: 3 decades of development. *Blood* **2009,** *113* (16), 3655-65.

12. Haussler, M.; Sidell, N.; Kelly, M.; Donaldson, C.; Altman, A.; Mangelsdorf, D., Specific high-affinity binding and biologic action of retinoic acid in human neuroblastoma cell lines. *Proc Natl Acad Sci U S A* **1983,** *80* (18), 5525-9.

13. Reynolds, C. P., Differentiating agents in pediatric malignancies: retinoids in neuroblastoma. *Curr Oncol Rep* **2000,** *2* (6), 511-8.

14. Matthay, K. K.; Villablanca, J. G.; Seeger, R. C.; Stram, D. O.; Harris, R. E.; Ramsay, N. K.; Swift, P.; Shimada, H.; Black, C. T.; Brodeur, G. M.; Gerbing, R. B.; Reynolds, C. P., Treatment of high-risk neuroblastoma with intensive chemotherapy, radiotherapy, autologous bone marrow transplantation, and 13-cis-retinoic acid. Children's Cancer Group. *N Engl J Med* **1999,** *341* (16), 1165-73.

15. Hirschmann-Jax, C.; Foster, A. E.; Wulf, G. G.; Nuchtern, J. G.; Jax, T. W.; Gobel, U.; Goodell, M. A.; Brenner, M. K., A distinct "side population" of cells with high drug efflux capacity in human tumor cells. *Proc Natl Acad Sci U S A* **2004,** *101* (39), 14228-33.

16. Reya, T.; Morrison, S. J.; Clarke, M. F.; Weissman, I. L., Stem cells, cancer, and cancer stem cells. *Nature* **2001,** *414* (6859), 105-11.

17. Bahmad, H. F.; Chamaa, F.; Assi, S.; Chalhoub, R. M.; Abou-Antoun, T.; Abou-Kheir, W., Cancer Stem Cells in Neuroblastoma: Expanding the Therapeutic Frontier. *Frontiers in Molecular Neuroscience* **2019,** *12* (131).

18. Hirschmann-Jax, C.; Foster, A. E.; Wulf, G. G.; Nuchtern, J. G.; Jax, T. W.; Gobel, U.; Goodell, M. A.; Brenner, M. K., A distinct “side population” of cells with high drug efflux capacity in human tumor cells. *Proceedings of the National Academy of Sciences of the United States of America* **2004,** *101* (39), 14228-14233.

19. Newton, T. C.; Wolcott, K.; Roberts, S. S., Comparison of the side populations in pretreatment and postrelapse neuroblastoma cell lines. *Transl Oncol* **2010,** *3* (4), 246-251.

20. Hansford, L. M.; McKee, A. E.; Zhang, L.; George, R. E.; Gerstle, J. T.; Thorner, P. S.; Smith, K. M.; Look, A. T.; Yeger, H.; Miller, F. D.; Irwin, M. S.; Thiele, C. J.; Kaplan, D. R., Neuroblastoma Cells Isolated from Bone Marrow Metastases Contain a Naturally Enriched Tumor-Initiating Cell. *Cancer Research* **2007,** *67* (23), 11234-11243.

21. Ding, S.; Schultz, P. G., A role for chemistry in stem cell biology. *Nature Biotechnology* **2004,** *22* (7), 833-840.

22. Brey, D. M.; Motlekar, N. A.; Diamond, S. L.; Mauck, R. L.; Garino, J. P.; Burdick, J. A., High-throughput screening of a small molecule library for promoters and inhibitors of mesenchymal stem cell osteogenic differentiation. *Biotechnol Bioeng* **2011,** *108* (1), 163-74.

23. Barbaric, I.; Jones, M.; Harley, D. J.; Gokhale, P. J.; Andrews, P. W., High-Content Screening for Chemical Modulators of Embryonal Carcinoma Cell Differentiation and Survival. 2011; Vol. 16, pp 603-617.

24. Heinis, C.; Rutherford, T.; Freund, S.; Winter, G., Phage-encoded combinatorial chemical libraries based on bicyclic peptides. *Nat Chem Biol* **2009,** *5* (7), 502-7.

25. Perron, A.; Nishikawa, Y.; Iwata, J.; Shimojo, H.; Takaya, J.; Kobayashi, K.; Imayoshi, I.; Mbenza, N. M.; Takenoya, M.; Kageyama, R.; Kodama, Y.; Uesugi, M., Small-molecule screening yields a compound that inhibits the cancer-associated transcription factor Hes1 via the PHB2 chaperone. *The Journal of biological chemistry* **2018,** *293* (21), 8285-8294.

26. Wei, W.; Ma, C.; Cao, Y.; Yang, L.; Huang, Z.; Qin, D.; Chen, Y.; Liu, C.; Xia, L.; Wang, T.; Lei, H.; Yu, Y.; Huang, M.; Tong, Y.; Xu, H.; Gao, F.; Zhang, J.; Wu, Y.-L., Identification of H7 as a novel peroxiredoxin I inhibitor to induce differentiation of leukemia cells. *Oncotarget* **2015,** *7* (4), 3873-3883.

27. Barbaric, I.; Gokhale, P. J.; Andrews, P. W., High-content screening of small compounds on human embryonic stem cells. *Biochemical Society transactions* **2010,** *38* (4), 1046-50.

28. Sykes, D. B.; Haynes, M. K.; Waller, A.; Garcia, M.; Ursu, O.; Gouveia, K. E.; Sklar, L.; Lewis, T. A.; Dandapani, S.; Munoz, B.; Scadden, D. T.; Palmer, M.; Schreiber, S. L., Discovering Small Molecules that Overcome Differentiation Arrest in Acute Myeloid Leukemia. In *Probe Reports from the NIH Molecular Libraries Program*, National Center for Biotechnology Information (US): Bethesda (MD), 2010.

29. Chauffert, B.; Dimanche-Boitrel, M. T.; Garrido, C.; Ivarsson, M.; Martin, M.; Martin, F.; Solary, E., New insights into the kinetic resistance to anticancer agents. *Cytotechnology* **1998,** *27* (1-3), 225-35.

30. Cheung, T. H.; Rando, T. A., Molecular regulation of stem cell quiescence. *Nature reviews. Molecular cell biology* **2013,** *14* (6), 329-340.

31. Wainwright, L. J.; Lasorella, A.; Iavarone, A., Distinct mechanisms of cell cycle arrest control the decision between differentiation and senescence in human neuroblastoma cells. *Proceedings of the National Academy of Sciences* **2001,** *98* (16), 9396-9400.

32. Sidell, N., Retinoic Acid-Induced Growth Inhibition and Morphologic Differentiation of Human Neuroblastoma Cells In Vitro2. *JNCI: Journal of the National Cancer Institute* **1982,** *68* (4), 589-596.

33. Sidell, N.; Altman, A.; Haussler, M. R.; Seeger, R. C., Effects of retinoic acid (RA) on the growth and phenotypic expression of several human neuroblastoma cell lines. *Experimental cell research* **1983,** *148* (1), 21-30.

34. Sidell, N.; Sarafian, T.; Kelly, M.; Tsuchida, T.; Haussler, M., Retinoic acid-induced differentiation of human neuroblastoma: a cell variant system showing two distinct responses. *Exp Cell Biol* **1986,** *54* (5-6), 287-300.

35. Zhao, Z.; Ma, X.; Hsiao, T.-H.; Lin, G.; Kosti, A.; Yu, X.; Suresh, U.; Chen, Y.; Tomlinson, G. E.; Pertsemlidis, A.; Du, L., A high-content morphological screen identifies novel microRNAs that regulate neuroblastoma cell differentiation. *Oncotarget* **2014,** *5* (9), 2499-2512.

36. Roukos, V.; Pegoraro, G.; Voss, T. C.; Misteli, T., Cell cycle staging of individual cells by fluorescence microscopy. *Nature protocols* **2015,** *10* (2), 334-48.

37. Soriano-Romaní, L.; García-Posadas, L.; López-García, A.; Paraoan, L.; Diebold, Y., Thrombospondin-1 induces differential response in human corneal and conjunctival epithelial cells lines under in vitro inflammatory and apoptotic conditions. *Experimental Eye Research* **2015,** *134*, 1-14.

38. Wongwananuruk, T.; Sato, T.; Kajihara, T.; Matsumoto, S.; Akita, M.; Tamura, K.; Brosens, J. J.; Ishihara, O., Endometrial androgen signaling and decidualization regulate trophoblast expansion and invasion in co-culture: A time-lapse study. *Placenta* **2016,** *47*, 56-62.

39. van Meerloo, J.; Kaspers, G. J. L.; Cloos, J., Cell Sensitivity Assays: The MTT Assay. In *Cancer Cell Culture: Methods and Protocols*, Cree, I. A., Ed. Humana Press: Totowa, NJ, 2011; pp 237-245.

40. Gaetano, C.; Manni, I.; Bossi, G.; Piaggio, G.; Soddu, S.; Farina, A.; Sacchi, A.; Helman, L. J., Retinoic acid and camp differentially regulate human chromogranin a promoter activity during differentiation of neuroblastoma cells. *European Journal of Cancer* **1995,** *31* (4), 447-452.

41. Ross, R.; Spengler, B.; Domenech, C.; Porubcin, M.; Rettig, W.; Biedler, J., Human neuroblastoma I-type cells are malignant neural crest stem cells. *Cell Growth Differ* **1995,** *6* (4), 449-456.

42. Walton, J. D.; Kattan, D. R.; Thomas, S. K.; Spengler, B. A.; Guo, H.-F.; Biedler, J. L.; Cheung, N.-K. V.; Ross, R. A., Characteristics of stem cells from human neuroblastoma cell lines and in tumors. *Neoplasia (New York, N.Y.)* **2004,** *6* (6), 838-845.

43. Rettig, W. J.; Spengler, B. A.; Chesa, P. G.; Old, L. J.; Biedler, J. L., Coordinate Changes in Neuronal Phenotype and Surface Antigen Expression in Human Neuroblastoma Cell Variants. *Cancer Research* **1987,** *47* (5), 1383-1389.

44. Preis, P. N.; Saya, H.; Nadasdi, L.; Hochhaus, G.; Levin, V.; Sadee, W., Neuronal cell differentiation of human neuroblastoma cells by retinoic acid plus herbimycin A. *Cancer Res* **1988,** *48* (22), 6530-4.

45. Shah, N.; Wang, J.; Selich-Anderson, J.; Graham, G.; Siddiqui, H.; Li, X.; Khan, J.; Toretsky, J., PBX1 is a favorable prognostic biomarker as it modulates 13-cis retinoic acid-mediated differentiation in neuroblastoma. *Clinical cancer research : an official journal of the American Association for Cancer Research* **2014,** *20* (16), 4400-4412.

46. Keshelava, N.; Seeger, R. C.; Groshen, S.; Reynolds, C. P., Drug Resistance Patterns of Human Neuroblastoma Cell Lines Derived from Patients at Different Phases of Therapy. *Cancer Research* **1998,** *58* (23), 5396-5405.

47. Keshelava, N.; Zuo, J. J.; Chen, P.; Waidyaratne, S. N.; Luna, M. C.; Gomer, C. J.; Triche, T. J.; Reynolds, C. P., Loss of p53 Function Confers High-Level Multidrug Resistance in Neuroblastoma Cell Lines. *Cancer Research* **2001,** *61* (16), 6185-6193.

48. Gaetano, C.; Matsumoto, K.; Thiele, C. J., Retinoic acid negatively regulates p34cdc2 expression during human neuroblastoma differentiation. *Cell Growth Differ* **1991,** *2* (10), 487-93.

49. Schubert, D.; Humphreys, S.; Baroni, C.; Cohn, M., In vitro DIFFERENTIATION OF A MOUSE NEUROBLASTOMA. *Proceedings of the National Academy of Sciences* **1969,** *64* (1), 316-323.

50. Schubert, D.; Humphreys, S.; de Vitry, F.; Jacob, F., Induced differentiation of a neuroblastoma. *Developmental Biology* **1971,** *25* (4), 514-546.

51. Rauvala, H., Neurite outgrowth of neuroblastoma cells: dependence on adhesion surface--cell surface interactions. *Journal of Cell Biology* **1984,** *98* (3), 1010-1016.

52. Schultz, A.; Larsson, C., Ceramide influences neurite outgrowth and neuroblastoma cell apoptosis regulated by novel protein kinase C isoforms. *Journal of Neurochemistry* **2004,** *89* (6), 1427-1435.

53. Henriksen, J.; Haug, B.; Buechner, J.; Tømte, E.; Løkke, C.; Flaegstad, T.; Einvik, C., Conditional expression of retrovirally delivered anti-MYCN shRNA as an in vitro model system to study neuronal differentiation in MYCN-amplified neuroblastoma. *BMC Dev Biol* **2011,** *11*, 1.

54. Kasim, M.; Hess, V.; Scholz, H.; Persson, P. B.; Faehling, M., Achaete-Scute Homolog 1 Expression Controls Cellular Differentiation of Neuroblastoma. 2016; Vol. 9.

55. Marangos, P. J.; Schmechel, D. E.; Parma, A. M.; Goodwin, F. K., Developmental profile of neuron-specific (NSE) and non-neuronal (NNE) enolase. *Brain Research* **1980,** *190* (1), 185-193.

56. Marangos, P. J.; Goodwin, F. K.; Parma, A.; Lauter, C.; Trams, E., Neuron specific protein (NSP) in neuroblastoma cells: Relation to differentiation. *Brain Research* **1978,** *145* (1), 49-58.

57. Odelstad, L.; P→hlman, S.; Nilsson, K.; Larsson, E.; Läckgren, G.; Johansson, K.-E.; Hjertén, S.; Grotte, G., Neuron-specific enolase in relation to differentiation in human neuroblastoma. *Brain Research* **1981,** *224* (1), 69-82.

58. Cheung, Y.-T.; Lau, W. K.-W.; Yu, M.-S.; Lai, C. S.-W.; Yeung, S.-C.; So, K.-F.; Chang, R. C.-C., Effects of all-trans-retinoic acid on human SH-SY5Y neuroblastoma as in vitro model in neurotoxicity research. *NeuroToxicology* **2009,** *30* (1), 127-135.

59. Naveen, C. R.; Gaikwad, S.; Agrawal-Rajput, R., Berberine induces neuronal differentiation through inhibition of cancer stemness and epithelial-mesenchymal transition in neuroblastoma cells. *Phytomedicine* **2016,** *23* (7), 736-744.

60. Luduena, R. F., Multiple forms of tubulin: different gene products and covalent modifications. *Int Rev Cytol* **1998,** *178*, 207-75.

61. Desai, A.; Mitchison, T. J., MICROTUBULE POLYMERIZATION DYNAMICS. *Annual Review of Cell and Developmental Biology* **1997,** *13* (1), 83-117.

62. Joshi, H. C.; Cleveland, D. W., Differential utilization of beta-tubulin isotypes in differentiating neurites. *J Cell Biol* **1989,** *109* (2), 663-673.

63. Skene, J. H., Axonal growth-associated proteins. *Annu Rev Neurosci* **1989,** *12*, 127-56.

64. Benowitz, L. I.; Routtenberg, A., GAP-43: an intrinsic determinant of neuronal development and plasticity. *Trends in Neurosciences* **1997,** *20* (2), 84-91.

65. Yankner, B. A.; Benowitz, L. I.; Villa-Komaroff, L.; Neve, R. L., Transfection of PC12 cells with the human GAP-43 gene: effects on neurite outgrowth and regeneration. *Molecular Brain Research* **1990,** *7* (1), 39-44.

66. Morton, A. J.; Buss, T. N., Accelerated Differentiation in Response to Retinoic Acid After Retrovirally Mediated Gene Transfer of GAP-43 into Mouse Neuroblastoma Cells. *European Journal of Neuroscience* **1992,** *4* (10), 910-916.

67. Raguenez, G.; Desire, L.; Lantrua, V.; Courtois, Y., BCL-2 Is Upregulated in Human SH-SY5Y Neuroblastoma Cells Differentiated by Overexpression of Fibroblast Growth Factor 1. *Biochemical and Biophysical Research Communications* **1999,** *258* (3), 745-751.

68. Acosta, S.; Lavarino, C.; Paris, R.; Garcia, I.; de Torres, C.; Rodríguez, E.; Beleta, H.; Mora, J., Comprehensive characterization of neuroblastoma cell line subtypes reveals bilineage potential similar to neural crest stem cells. *BMC Dev Biol* **2009,** *9*, 12-12.

69. Edsjö, A.; Nilsson, H.; Vandesompele, J.; Karlsson, J.; Pattyn, F.; Culp, L. A.; Speleman, F.; Påhlman, S., Neuroblastoma cells with overexpressed MYCN retain their capacity to undergo neuronal differentiation. *Laboratory Investigation* **2004,** *84* (4), 406-417.

70. Verhaagen, J.; Hermens, W. T. J. M. C.; Oestreicher, A. B.; Gispen, W. H.; Rabkin, S. D.; Pfaff, D. W.; Kaplitt, M. G., Expression of the growth-associated protein B-50/GAP43 via a defective herpes-simplex virus vector results in profound morphological changes in non-neuronal cells. *Molecular Brain Research* **1994,** *26* (1), 26-36.

71. Widmer, F.; Caroni, P., Phosphorylation-site mutagenesis of the growth-associated protein GAP-43 modulates its effects on cell spreading and morphology. *Journal of Cell Biology* **1993,** *120* (2), 503-512.

72. Zhang, D.; Babayan, L.; Ho, H.; Heaney, A. P., Chromogranin A regulates neuroblastoma proliferation and phenotype. *Biol Open* **2019,** *8* (3).

73. Abemayor, E.; Sidell, N., Human neuroblastoma cell lines as models for the in vitro study of neoplastic and neuronal cell differentiation. *Environmental health perspectives* **1989,** *80*, 3-15.

74. Reynolds, C. P.; Wang, Y.; Melton, L. J.; Einhorn, P. A.; Slamon, D. J.; Maurer, B. J., Retinoic-acid-resistant neuroblastoma cell lines show altered MYC regulation and high sensitivity to fenretinide. *Med Pediatr Oncol* **2000,** *35* (6), 597-602.

75. Ponzoni, M.; Bocca, P.; Chiesa, V.; Decensi, A.; Pistoia, V.; Raffaghello, L.; Rozzo, C.; Montaldo, P. G., Differential effects of N-(4-hydroxyphenyl) retinamide and retinoic acid on neuroblastoma cells: apoptosis versus differentiation. *Cancer research* **1995,** *55* (4), 853-861.

76. Reynolds, C. P., Differentiating agents in pediatric malignancies: retinoids in neuroblastoma. *Current oncology reports* **2000,** *2* (6), 511-518.

77. Cuperus, R.; Tytgat, G. A.; Leen, R.; Brites, P.; Bras, J.; Caron, H. N.; Van Kuilenburg, A. B., Pleiotropic effects of fenretinide in neuroblastoma cell lines and multicellular tumor spheroids. *International journal of oncology* **2008,** *32* (5), 1011-1019.

78. Siegel, T. N.; Hekstra, D. R.; Cross, G. A. M., Analysis of the Trypanosoma brucei cell cycle by quantitative DAPI imaging. *Mol Biochem Parasitol* **2008,** *160* (2), 171-174.

79. Darzynkiewicz, Z.; Juan, G., DNA Content Measurement for DNA Ploidy and Cell Cycle Analysis. *Current Protocols in Cytometry* **1997,** *00* (1), 7.5.1-7.5.24.

80. Dimri, G. P.; Lee, X.; Basile, G.; Acosta, M.; Scott, G.; Roskelley, C.; Medrano, E. E.; Linskens, M.; Rubelj, I.; Pereira-Smith, O.; et al., A biomarker that identifies senescent human cells in culture and in aging skin in vivo. *Proceedings of the National Academy of Sciences of the United States of America* **1995,** *92* (20), 9363-9367.

81. Debacq-Chainiaux, F.; Erusalimsky, J. D.; Campisi, J.; Toussaint, O., Protocols to detect senescence-associated beta-galactosidase (SA-βgal) activity, a biomarker of senescent cells in culture and in vivo. *Nature protocols* **2009,** *4* (12), 1798-1806.

82. Clark, O.; Daga, S.; Stoker, A. W., Tyrosine phosphatase inhibitors combined with retinoic acid can enhance differentiation of neuroblastoma cells and trigger ERK- and AKT-dependent, p53-independent senescence. *Cancer Letters* **2013,** *328* (1), 44-54.

83. Forster, J. I.; Köglsberger, S.; Trefois, C.; Boyd, O.; Baumuratov, A. S.; Buck, L.; Balling, R.; Antony, P. M. A., Characterization of Differentiated SH-SY5Y as Neuronal Screening Model Reveals Increased Oxidative Vulnerability. *J Biomol Screen* **2016,** *21* (5), 496-509.

84. Marler, K. J. M.; Kozma, R.; Ahmed, S.; Dong, J.-M.; Hall, C.; Lim, L., Outgrowth of neurites from NIE-115 neuroblastoma cells is prevented on repulsive substrates through the action of PAK. *Molecular and cellular biology* **2005,** *25* (12), 5226-5241.

85. Wlodkowic, D.; Skommer, J.; Darzynkiewicz, Z., Flow cytometry-based apoptosis detection. In *Apoptosis*, Springer: 2009; pp 19-32.

86. Kroemer, G.; Martin, S. J., Caspase-independent cell death. *Nat Med* **2005,** *11* (7), 725-30.

87. Leist, M.; Jäättel, M., FOUR DEATHS AND A FUNERAL: FROM CASPASES TO ALTERNATIVE MECHANISMS. *Nature Reviews Molecular Cell Biology* **2001,** *2* (8), 589-598.

88. Wlodkowic, D.; Skommer, J.; Darzynkiewicz, Z., Flow Cytometry-Based Apoptosis Detection. In *Apoptosis: Methods and Protocols, Second Edition*, Erhardt, P.; Toth, A., Eds. Humana Press: Totowa, NJ, 2009; pp 19-32.

89. Aird, K. M.; Zhang, R., Detection of senescence-associated heterochromatin foci (SAHF). In *Cell Senescence*, Springer: 2013; pp 185-196.